Determining the Properties of Low-frequency Farley-Buneman Waves at High Latitudes

by

Josef Drexler

Department of Physics and Astronomy

Graduate Program in Physics

Submitted in partial fulfilment

of the requirements for the degree of

Master of Science

Faculty of Graduate Studies

The University of Western Ontario

London, Ontario

April 2000

Abstract

The growth rate of low-frequency Farley-Buneman waves is so small that the instability switches from absolute to convective. The inhomogeneity of the medium then has to be taken into account for a proper description of the wave evolution.

In Fourier analysis this means that the eigenfrequency is a function of position which requires a mode-coupling formalism. Alternatively, one can shy away from Fourier analysis and use a WKB type description by considering the instantaneous phase and amplitude of a particular wave train which is then allowed to grow and propagate. One result from this is that the parallel wavenumber is a predictable function of time and space and not a free parameter.

I have simulated the wave evolution by using a numerically stable ray-tracing algorithm. This has allowed me to determine the spectrum of a particular wave train without having to resort to Fourier analysis at all.

Keywords: Farley-Buneman waves, Ionospheric Irregularities, Nonlocal convective plasma instabilities

Acknowledgement

I would like to express my deepest thanks to Dr. Jean-Pierre St.-Maurice, the supervisor of this study, for his ongoing support, enthusiasm, dedication, and the invaluable amount of advice and helpful suggestions he was always ready to offer.

I would also like to thank the members of my advisory committee, Dr. R.J. Sica and Dr. S.R. Valluri, for their suggestions and guidance which helped me complete this work.

I gratefully acknowledge the discussions I had with the other members of the space and atmospheric physics group, particularly Dr. D.R. Moorcroft, Dr. Randy Kissack and Dr. P.T. Jayachandran, which always proved insightful and interesting.

Finally I want to thank my family, my parents and my brothers, for their much needed support during the course of this study, as well as my friend Volker Gimple for his support and loyalty across continents.

Dedicated to my parents.

Table of Contents

List of Figures

Chapter 1

INTRODUCTION

1.1 The Ionosphere

The ionosphere for the Earth begins at about 70 km altitude. Its characteristic is being ionized, and it behaves like a collisional plasma, with the importance of collisions depending on the altitude, through the exponential decay in neutral density. It has three distinctive regions:

D-region, from 70 90 km. This is the region where the plasma density becomes measurable. However, the neutral density is still very large, so that electrons and ions have a large collision frequency. Although there is a plasma density, these collisions with the neutrals make ions and electrons behave like the neutral atmosphere.

E-region, from 90 150 km. Here, the neutral density becomes so small that the electron-neutral collision frequency is much smaller than the electron's Larmor frequency $\Omega_L = eB/m_e$, so that the electrons can follow the $\mathbf{E} \times \mathbf{B}$ drift. The ions on the other hand follow the neutral gas because of their smaller Larmor

frequency for altitudes up to about 120 km. Above 120 km the collision frequencies become small enough even for the ions, and they start $\mathbf{E} \times \mathbf{B}$ drifting too.

F-region, from 150 -500 km. In this region, the neutral density is very small, and both electrons and ions are mostly free of collisions.

The irregularities this thesis deals with, Farley-Buneman waves, are excited by a Hall current in the E-region, therefore it is worthwhile to have a closer look at this region.

1.2 The E Region

In this region, electrons are $\mathbf{E} \times \mathbf{B}$-drifting and ions follow the neutral wind. This creates a Hall current perpendicular to $\mathbf{B}$ that enables Farley-Buneman instabilities to grow, so it is useful to look at it more thoroughly.

As mentioned in section 1.1, the E-region extends from 90 km to 150 km. At these altitudes, the neutral density has fallen sufficiently to allow electrons to move with very few collisions compared to their gyro-frequency. The temperature increases steadily from about 100 K at the bottom of the E-region up to a maximum value between 600 K and 1000 K at the top, depending on solar activity. This increase in temperature is due to the absorption of solar UV radiation, which also contributes to the increase in plasma density.

This plasma density is typically of the order of 10^{11} m^{-3}, which is a relatively small value compared to the neutral density of about 10^{17} m^{-3}. However, the important conditions for plasma behavior are still met, as the Debye length is to the order of 0.1 cm, and consequently the number of particles in a Debye sphere N_D is about 10^4.

From the large N_D we can see that it really is a plasma, however only the electrons have a small enough collision frequency ν_e and can $\mathbf{E}\times\mathbf{B}$ drift. Thus, the electrons are "magnetized" because ν_e is much less than their cyclotron frequency Ω_e, whereas the ions have $\nu_i \geq \Omega_i$ for most of the E-region, so that they mostly follow the neutral gas, i.e. they are collisional. It is only above about 120 km that the collision frequency ν_i is low enough and the ions start $\mathbf{E}\times\mathbf{B}$ drifting too.

1.3 Electron and Ion motion

In the plane perpendicular to $\mathbf{B}$, it is only the balance between collisions and electromagnetic forces that matters, all other forces are negligible. Therefore, the steady state ion and electron equations of motion are in this case

$$0 = n_i e(\mathbf{E} - \mathbf{v}_i \times \mathbf{B}) - \rho_i \nu_{in}(\mathbf{v}_i - \mathbf{v}_n) \tag{1.3.1}$$

$$0 = -n_e e(\mathbf{E} - \mathbf{v}_e \times \mathbf{B}) - \rho_e \nu_{en}(\mathbf{v}_e - \mathbf{v}_n) \tag{1.3.2}$$

From this we get for the ions

$$\frac{\nu_{in}}{\Omega_i}(\mathbf{v}_i - \mathbf{v}_n) = \frac{\mathbf{E}}{B} - \frac{\mathbf{v}_i \times \mathbf{B}}{B} \tag{1.3.3}$$

and

$$\frac{\nu_{in}}{\Omega_i}\mathbf{v}_{in} = \frac{\mathbf{E}_0}{B} - \frac{\mathbf{v}_{in} \times \mathbf{B}}{B} \tag{1.3.4}$$

where

$$\Omega_i = \frac{eB}{m_i} \tag{1.3.5}$$

$$\mathbf{E}_0 = \mathbf{E} - \mathbf{v}_n \times \mathbf{B} \tag{1.3.6}$$

$$\mathbf{v}_{in} = \mathbf{v}_i - \mathbf{v}_n \tag{1.3.7}$$

To get an expression for $\mathbf{v}_{in} \times \mathbf{B}$, we take the cross product of equation (1.3.4) with $\mathbf{B}$ and get:

$$\frac{\mathbf{v}_{in} \times \mathbf{B}}{B} = \frac{\Omega_i}{\nu_{in}} \frac{\mathbf{E}_0 \times \mathbf{B}}{B^2} - \frac{\Omega_i}{\nu_{in}} \mathbf{v}_{in} \tag{1.3.8}$$

which we can put into (1.3.4) to obtain

$$\frac{\nu_{in}^2}{\Omega_i^2} \mathbf{v}_{in} = \frac{\nu_{in}}{\Omega_i} \frac{\mathbf{E}_0}{B} - \frac{\mathbf{E}_0 \times \mathbf{B}}{B^2} - \mathbf{v}_{in} \tag{1.3.9}$$

or

$$\mathbf{v}_i = \mathbf{v}_n - \frac{\frac{\nu_{in}}{\Omega_i}}{1 - \frac{\nu_{in}^2}{\Omega_i^2}} \frac{\mathbf{E}_0}{B} - \frac{1}{1 - \frac{\nu_{in}^2}{\Omega_i^2}} \frac{\mathbf{E}_0 \times \mathbf{B}}{B^2} \tag{1.3.10}$$

and the corresponding equation for the electrons

$$\mathbf{v}_e = \mathbf{v}_n - \frac{\frac{\nu_{en}}{\Omega_e}}{1 - \frac{\nu_{en}^2}{\Omega_e^2}} \frac{\mathbf{E}_0}{B} - \frac{1}{1 - \frac{\nu_{en}^2}{\Omega_e^2}} \frac{\mathbf{E}_0 \times \mathbf{B}}{B^2} \tag{1.3.11}$$

However, in the E-region, we have ν_e, Ω_i very small for the electrons, and Ω_i, ν_i very small for the ions, so that the velocities can be approximated as

$$\mathbf{v}_e \approx \mathbf{v}_n - \frac{\mathbf{E}_0 \times \mathbf{B}}{B^2} = \frac{\mathbf{E} \times \mathbf{B}}{B^2} \tag{1.3.12}$$

$$\mathbf{v}_i \approx \mathbf{v}_n - \frac{\Omega_i}{\nu_i} \frac{\mathbf{E}_0}{B} \tag{1.3.13}$$

Therefore, electrons $\mathbf{E} \times \mathbf{B}$ drift and ions mostly follow the neutrals, with a small component in the $\mathbf{E}_0$ direction. This difference in electron and ion velocity has an important consequence, which is a Hall current in the $\mathbf{E} \times \mathbf{B}$ direction. This current is a source of free energy, and can then be used to excite waves in order to dissipate this energy. These waves are the Farley-Buneman instabilities.

1.4 Farley-Buneman Waves

The following linear model of traditional, "local" Farley-Buneman waves (see *Farley*, 1963; *Buneman*, 1963) was developed by J.-P. St-Maurice. Its originality lies in the fact that it can explain the waves without having to do a Fourier analysis, which makes it easier for some to understand the physics behind the waves.

We will assume that the electric field $\mathbf{E}_0$ is perpendicular to $\mathbf{B}$. This is usually the case in the E-region, because parallel electric fields can easily be shorted out by the electrons. We then choose the $\mathbf{E}_0 \times \mathbf{B}$ direction to be the x direction, z is along the magnetic field lines, which is true at high latitudes.

1.5 Motion of the waves

First, we want to concentrate on the motion of the waves, and derive the velocity. Then, we can later add terms that determine growth or decay of the waves.

The model behind this derivation is actually quite simple. Suppose there is a clump in plasma density, a local enhancement with an arbitrary shape $\delta n / n_0 = f(x)$ as illustrated in figure 1.1.

We will show that it propagates in the direction of the current. Actually, this derivation is in terms of the $\mathbf{E}_0 \times \mathbf{B}$ drift rather than the current, but both are equivalent, and the derivation can easily be generalized to other currents.

The electrons in the clump are $\mathbf{E} \times \mathbf{B}$ drifting, while the ions stay behind because they are collisional. This creates an additional electric field $\delta\mathbf{E}$, which accelerates the ions, and decelerates the electrons in the $\mathbf{E}_0 \times \mathbf{B}$ direction, thus trying to restore the equilibrium. We can determine the resulting perturbed ion velocity from

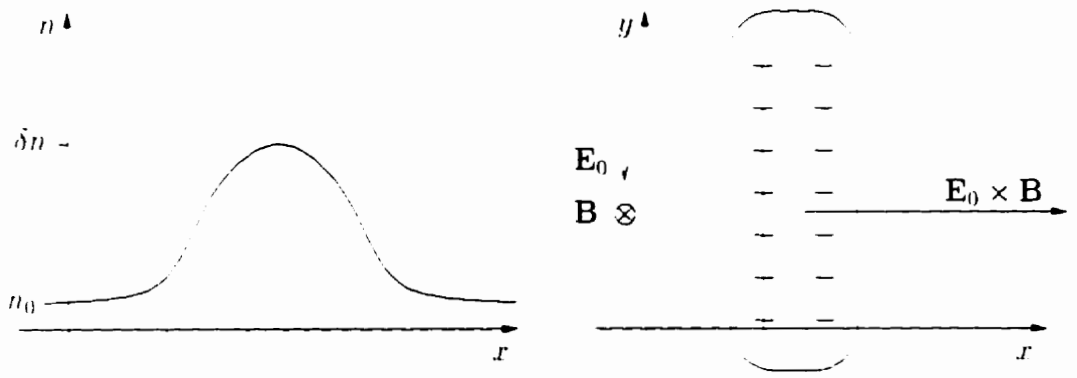

Figure 1.1: A clump in plasma density

equation (1.3.10) to be

$$\mathbf{v}_i - \delta\mathbf{v}_i = \mathbf{v}_n - \frac{\frac{\nu_{in}}{\Omega_i}}{1-\frac{\nu_{in}^2}{\Omega_i^2}}\frac{\mathbf{E}_0-\delta\mathbf{E}}{B} - \frac{1}{1-\frac{\nu_{in}^2}{\Omega_i^2}}\frac{(\mathbf{E}_0-\delta\mathbf{E})\times\mathbf{B}}{B^2} \tag{1.5.1}$$

From this we can see that the velocity perturbation for electrons and ions is given by

$$\delta\mathbf{v}_i = \frac{\frac{\nu_{in}}{\Omega_i}}{1-\frac{\nu_{in}^2}{\Omega_i^2}}\frac{\delta\mathbf{E}}{B} - \frac{1}{1-\frac{\nu_{in}^2}{\Omega_i^2}}\frac{\delta\mathbf{E}\times\mathbf{B}}{B^2} \tag{1.5.2}$$

$$\delta\mathbf{v}_e = \frac{\frac{\nu_{en}}{\Omega_e}}{1-\frac{\nu_{en}^2}{\Omega_e^2}}\frac{\delta\mathbf{E}}{B} - \frac{1}{1-\frac{\nu_{en}^2}{\Omega_e^2}}\frac{\delta\mathbf{E}\times\mathbf{B}}{B^2} \tag{1.5.3}$$

Considering only the $\mathbf{E}\times\mathbf{B}$ direction, which we define to be the x axis, we find that

$$\delta v_i = \frac{\Omega_i}{\nu_i}\frac{\delta E}{B} \tag{1.5.4}$$

$$\delta v_e = -\frac{\nu_e}{\Omega_e}\frac{\delta E}{B} \tag{1.5.5}$$

The equation of continuity for electrons and ions in this direction is then given by

$$\frac{\partial n_e}{\partial t} = -\frac{\partial}{\partial x}(n_e v_e) \tag{1.5.6}$$

$$\frac{\partial n_i}{\partial t} = -\frac{\partial}{\partial x}(n_i v_i) \tag{1.5.7}$$

Because a plasma has to remain electrically neutral ($n_e = n_i = n$), we can see that

$$\delta(n_i v_i) = \delta(n_e v_e) \tag{1.5.8}$$

$$n_0 \delta v_i - n_0 \delta v_e - v_e \delta n = 0 \tag{1.5.9}$$

The missing term $v_i \delta n$ is negligible, because ions are collisional and have a negligible velocity relative to the neutrals. Combining this with equations (1.5.4) and (1.5.5), we get

$$v_e \frac{\delta n}{n_0} = \delta v_i - \delta v_e = \frac{\delta E}{B}\left[\frac{\Omega_i}{\nu_i} - \frac{\nu_e}{\Omega_e}\right] \tag{1.5.10}$$

$$\frac{\delta n}{n_0} = \frac{\Omega_i}{\nu_i}(1 - \Psi)\frac{\delta E}{E_0} \tag{1.5.11}$$

where

$$\Psi = \frac{\nu_i}{\Omega_i}\frac{\nu_e}{\Omega_e} < 1 \tag{1.5.12}$$

Taking (1.5.4) into (1.5.7), and replacing δE with the value from (1.5.11), we get

$$\frac{\partial \delta n}{\partial t} = -\frac{\partial}{\partial x}\left(n_0 \frac{\Omega_i}{\nu_i}\frac{\delta E}{B}\right) = -n_0 \frac{\partial}{\partial x}\left(\frac{1}{1-\Psi}\frac{\delta n}{n_0}\right)\frac{E_0}{B} \tag{1.5.13}$$

With the electron-ion drift $v_D = E_0 / B$, we can write this as

$$\frac{\partial}{\partial t}\frac{\delta n}{n_0} = -\frac{v_D}{1-\Psi}\frac{\partial}{\partial x}\left(\frac{\delta n}{n_0}\right) \tag{1.5.14}$$

or, in a more intuitive way

$$\left[\frac{\partial}{\partial t} - V\frac{\partial}{\partial x}\right]\frac{\delta n}{n_0} = 0 \tag{1.5.15}$$

This is the equation for a wave traveling with the velocity

$$V = \frac{v_D}{1-\Psi} = \frac{E_0 / B}{1-\Psi} \tag{1.5.16}$$

and the solution is simply the traveling clump:

$$\frac{\delta n}{n_0} = f(x - Vt) \tag{1.5.17}$$

It is here that the advantage of not using Fourier transforms becomes obvious, because equation (1.5.17) immediately tells us that the clump is moving, that it retains its initial shape, and what the velocity is. And even the dispersion relation can easily be read from equation (1.5.15). By writing $\partial/\partial t = -i\omega$ and $\partial/\partial x = ik$, we get

$$\omega - Vk = 0 \tag{1.5.18}$$

which shows that this is indeed a traveling, non-dispersive wave.

1.6 Growth and Decay

The effects which cause growth and decay of the wave are ion inertia and a pressure gradient, respectively. Ion inertia makes the slow ions pile up at the end of the clump where the ion density is already enhanced, so that the additional electric field $\delta\mathbf{E}$ becomes even larger, thus increasing the wave amplitude. This is somewhat ironic, because the ions are trying to catch up with the electrons in order to reduce the electric field and restore equilibrium, but they are too slow and pile up in a region with an increased ion density. Therefore the ions increase the electric field instead of decreasing it, and through this they make the wave unstable and grow.

The decay on the other hand comes from the pressure gradient which the local increase in density creates, and diffusion because of this pressure gradient makes the wave decay.

For a wave propagating in the plane perpendicular to $\mathbf{B}$, diffusion will act in the x and the y directions, therefore it is convenient to write the ion equation of motion

using vectors:

$$\frac{\partial \mathbf{v}_i}{\partial t} - \frac{e\delta\mathbf{E}}{m_i} = -\nu_i \mathbf{v}_i - \frac{\nabla p}{n_0 m_i} \tag{1.6.1}$$

Remembering that $\Omega_i = eB/m_i$ and $p = nKT_i$, we get

$$\frac{\partial \mathbf{v}_i}{\partial t} - \frac{\delta\mathbf{E}}{B}\Omega_i = -\nu_i \mathbf{v}_i - c_i^2 \nabla \frac{\delta n}{n_0} \tag{1.6.2}$$

where $c_i^2 = kT_i/m_i$ is the "ion-acoustic" speed of the ions. Taking the divergence of (1.6.2), we get

$$\nabla \cdot \left[\frac{\partial \delta \mathbf{v}_i}{\partial t} - \nu_i \delta \mathbf{v}_i \right] = \Omega_i \nabla \cdot \frac{\delta \mathbf{E}}{B} - c_i^2 \nabla^2 \frac{\delta n}{n_0} \tag{1.6.3}$$

and, with the ion equation of continuity,

$$-\frac{\partial^2}{\partial t^2}\frac{\delta n}{n_0} - \nu_i \frac{\partial}{\partial t}\frac{\delta n}{n_0} = \Omega_i \nabla \cdot \frac{\delta \mathbf{E}}{B} - c_i^2 \nabla^2 \frac{\delta n}{n_0} \tag{1.6.4}$$

We can find an expression for the electric field perturbation $\delta\mathbf{E}$ by looking at the electron equation of continuity:

$$\frac{\partial}{\partial t}\delta n = -\mathbf{v}_e \cdot \nabla \delta n - n_0 \nabla \cdot \delta \mathbf{v}_e \tag{1.6.5}$$

Because we now allow diffusion, we have to add the appropriate term to equation (1.5.5) and get

$$\delta \mathbf{v}_e = \frac{\nu_e}{\Omega_e}\left[-\frac{\delta\mathbf{E}}{B} - \frac{\nabla p}{n_0 m_e} \right] \tag{1.6.6}$$

Taking the divergence of (1.6.6) and using (1.6.5), we find that

$$\nabla \cdot \frac{\delta \mathbf{E}}{B} = \frac{\Omega_e}{\nu_e}\left[\frac{\partial}{\partial t} - \mathbf{v}_e \cdot \nabla \right] \frac{\delta n}{n_0} - \frac{\Omega_e}{\nu_e} c_e^2 \nabla^2 \frac{\delta n}{n_0} \tag{1.6.7}$$

where $c_e^2 = kT_e/m_e$. This can be combined with (1.6.4) to give us

$$-\frac{\Psi}{\nu_i}\frac{\partial^2}{\partial t^2}\frac{\delta n}{n_0} = (1-\Psi)\frac{\partial}{\partial t}\frac{\delta n}{n_0} - \mathbf{v}_e \cdot \nabla \frac{\delta n}{n_0} - \frac{\Psi}{\nu_i} c_e^2 \nabla^2 \frac{\delta n}{n_0} \tag{1.6.8}$$

where $c_s^2 = [k(T_e - T_i)]/m_i$ is the ion-acoustic speed of the plasma. Then, we have

$$\left[\frac{\partial}{\partial t} - \frac{\mathbf{v}_e}{1-\Psi}\cdot\nabla\right]\frac{\delta n}{n_0} = -\frac{\Psi}{\nu_i(1-\Psi)}\left[\frac{\partial^2}{\partial t^2}\frac{\delta n}{n_0} - c_s^2\nabla^2\frac{\delta n}{n_0}\right] \tag{1.6.9}$$

Because we take $\delta\mathbf{E}$ to be in the x direction, we can write (1.6.9) in the form

$$\frac{D}{Dt}f = -A\left[\frac{\partial^2}{\partial t^2} - c_s^2\frac{\partial^2}{\partial x^2}\right]f - Ac_s^2\frac{\partial^2}{\partial y^2}f \tag{1.6.10}$$

where

$$\frac{D}{Dt} = \frac{\partial}{\partial t} - V\frac{\partial}{\partial x} \tag{1.6.11}$$

is the convective derivative, or the time derivative when following the wave with velocity $V = (E \times B)/(1-\Psi)$. The growth constant A is given by

$$A = \frac{\Psi}{\nu_i(1-\Psi)} \tag{1.6.12}$$

Because both the first and the second time derivatives are present in (1.6.10), a multi-scaling expansion can be used to solve it. This is equivalent to assuming a solution with two independent time scales, one ($\tau = t$) for the fast wave oscillations and one ($\tau_g = \epsilon t$) for the growth of the wave. The small constant ϵ means that τ has to be long for τ_g to be felt. Therefore we can split (1.6.12) into two parts, one for each time scale:

$$f = f_0(\tau, \tau_g) - \epsilon f_1(\tau, \tau_g) \tag{1.6.13}$$

and the time derivative becomes

$$\frac{\partial}{\partial t} = \frac{\partial}{\partial \tau}\frac{\partial \tau}{\partial t} - \frac{\partial}{\partial \tau_g}\frac{\partial \tau_g}{\partial t} \tag{1.6.14}$$

$$= \frac{\partial}{\partial \tau} - \epsilon\frac{\partial}{\partial \tau_g} \tag{1.6.15}$$

The fast time scale is just the wave equation without growth

$$\left[\frac{\partial}{\partial \tau} - V\frac{\partial}{\partial x}\right]f_0 = 0 \tag{1.6.16}$$

But for f_1, we also have growth, and we get to first order in ϵ

$$\left[\frac{\partial}{\partial\tau} - V\frac{\partial}{\partial x}\right] f_1 - \frac{\partial}{\partial\tau_g} f_0 = A\left[c_s^2\frac{\partial^2}{\partial x^2} - \frac{\partial^2}{\partial\tau^2}\right] f_0 - Ac_s^2\frac{\partial^2}{\partial y^2} f_0 \tag{1.6.17}$$

$$\left[\frac{\partial}{\partial\tau} - V\frac{\partial}{\partial x}\right] f_1 = -\frac{\partial}{\partial\tau_g} f_0 - A\left[c_s^2\frac{\partial^2}{\partial x^2} - \frac{\partial^2}{\partial\tau^2}\right] f_0 - Ac_s^2\frac{\partial^2}{\partial y^2} f_0 \tag{1.6.18}$$

f_0 is an eigenvalue of f_1 because f_1 also contains the wave motion itself in addition to growth or decay, which means that the right hand side has to be zero, or f_1 would grow indefinitely, so that we have

$$\frac{\partial}{\partial\tau_g} f_0 = A(c_s^2 - V^2)\frac{\partial^2}{\partial x^2} f_0 - Ac_s^2\frac{\partial^2}{\partial y^2} f_0 \tag{1.6.19}$$

This is the equation for the growth of the wave. In the y direction it is a simple diffusion equation, but in the x direction there is one important difference. In the case of a wave propagating only in the x direction, the diffusion coefficient is $D = A(c_s^2 - V^2)$ and can be either positive or negative, depending on the wave speed V. If $V < c_s$, it is just ordinary diffusion, and the wave decays because the pressure gradient is stronger than the ion inertia effects.

However, for $V > c_s$ the diffusion constant is negative, so that we have "anti-diffusion": ion inertia increases the amplitude of the wave.

More generally, consider a wave train propagating at an angle θ to the $\mathbf{E} \times \mathbf{B}$ drift, but still in the x-y plane. This angle is called the "flow angle". Then, the wave vector is given by

$$k_x = k\cos\theta \qquad k_y = k\sin\theta \tag{1.6.20}$$

We can now write (1.6.19) in the form

$$\frac{\partial \ln f_0}{\partial\tau_g} = \gamma \tag{1.6.21}$$

with the growth rate γ being

$$\gamma = -A(c_s^2 - V^2)k_x^2 - Ac_s^2 k_y^2 = -Ak^2(c_s^2 - V^2\cos^2\theta) \qquad (1.6.22)$$

$$\gamma = \frac{(\omega^2 - k^2 c_s^2)\Psi}{(1-\Psi)\nu_i} \qquad (1.6.23)$$

where $\omega = kV\cos\theta$. This means that for a wave in the x-y plane, we can only have growth if $V\cos\theta > c_s$.

1.7 Altitude Effects

Now, consider a wave train which extends over a range of altitudes. Different altitudes have a different Ψ factor, because the collision frequencies decrease with height. From the dispersion relation (1.5.18) we can see that this implies a changing wave frequency, or a changing wave number. We will consider k to be fixed, because these waves are observed with radars using a constant wavelength, and let ω change with altitude instead. This changing frequency will mean, that after some time adjacent altitudes of the same wave train will be out of phase, as illustrated by figure 1.2.

This phase difference then leads to the development of a vertical structure in the wave, and the wave starts to propagate upwards in altitude. The vertical structure is equivalent to a z component of the wave vector, usually labeled k_z. The angle α between the plane perpendicular to $\mathbf{B}$ and the wave vector, with

$$\tan\alpha = \frac{k_\perp}{k_z} \quad \text{or, for small } k: \quad \alpha \approx \frac{k_\perp}{k_z} \qquad (1.7.1)$$

is called "aspect angle".

The aspect angle has usually been taken to be a free parameter to the Farley-Buneman problem, [e.g. *Schlegel*, 1996]. This has of course led to the question as

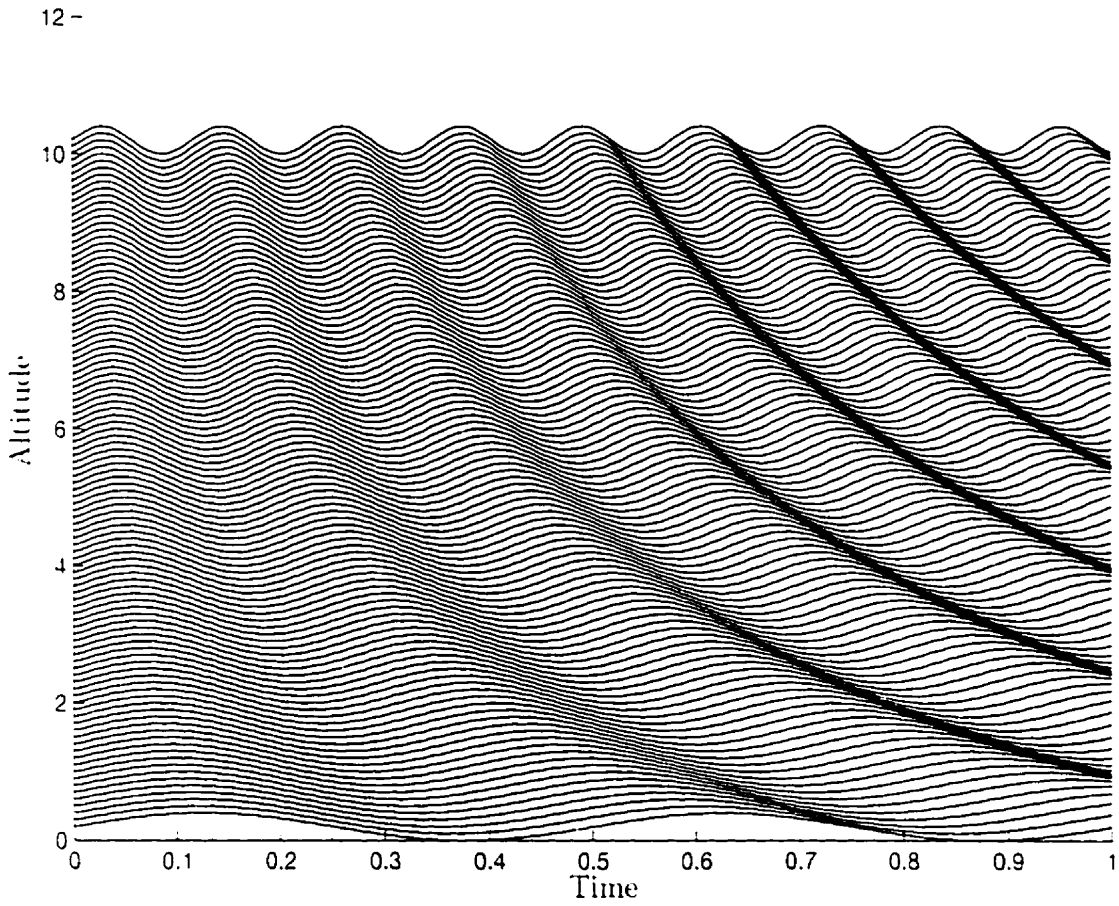

Figure 1.2: Example wave train plot demonstrating how vertical structure can appear as result from a non-uniform frequency (units are arbitrary)

to what value one should use for it, since it cannot be measured readily. However, with a non-local theory [*St.-Maurice*, 1985] which takes into account the non-uniform frequency and the spatial extent of the waves, the aspect angle becomes a predictable function of time and space. For example in figure 1.2, the aspect angle is zero initially but then evolves into a non-zero value. One such theory will be shown in the next chapter.

Chapter 2

NON-LOCAL DESCRIPTION

This chapter serves to highlight the derivation of an equation for the growth of the waves, and the relationship between frequency and parallel wave number as done by *Chen* [1996]. These results form the basis of the problem solved using the methods presented in this thesis.

2.1 Basic derivation

The starting point is the differential equation that describes the density perturbation, which can be found in many papers, [e. g. *Sudan*, 1983]. It is fundamentally the same procedure which was described in section 1.4 except for the presence of additional terms describing the vertical structure.

Donglei Chen's resulting equation for the density perturbation is

$$\frac{\partial^2}{\partial z^2}\left(\frac{\partial^2}{\partial t'^2}-\nu_i\frac{\partial}{\partial t'}-k^2c_s^2\right)\frac{\delta n}{n_0} - \frac{k^2\nu_e^2}{\Omega_e^2}\left[\frac{\partial^2}{\partial t'^2}-\nu_i\left(1-\frac{1}{\Psi_0'}\right)\frac{\partial}{\partial t'}-k^2c_s^2-\frac{i\nu_i}{\Psi_0'}\mathbf{k}\cdot\mathbf{v}_D\right]\frac{\delta n}{n_0}=0 \quad (2.1.1)$$

where

$$\Psi_0 = \frac{\nu_e \nu_i}{\Omega_e \Omega_i}, \qquad \Psi_0' = \Psi_0 \frac{k^2}{k^2} \tag{2.1.2}$$

$$\frac{\partial}{\partial t'} = \frac{\partial}{\partial t} + i\mathbf{k}_\sim \cdot \mathbf{v}_i \tag{2.1.3}$$

$$\mathbf{v}_D = \mathbf{v}_e - \mathbf{v}_i \tag{2.1.4}$$

As shown in section 1.7, the solution cannot have a simple plane wave decomposition, because the collision frequencies as well as $\mathbf{v}_D$ are changing with altitude.

2.2 Modified WKB Approach

The WKB approach is often used to solve a problem which has no strict plane wave decomposition. The particular approach Donglei Chen used in his thesis is to write the density fluctuation in the form

$$\frac{\delta n}{n_0} = A(z,t)\exp[iS(z,t)] \tag{2.2.1}$$

with amplitude A and phase S. A difference with the standard WKB method is that both A and S are assumed to be real, so that growth and decay are modeled through a changing amplitude as opposed to an imaginary part of the phase. This assumes that the derivatives of the amplitude in time and space are much smaller than those of the phase.

Once the phase is defined to be real, the instantaneous frequency and parallel wave number can be defined as

$$\omega = -\frac{\partial S}{\partial t} \tag{2.2.2}$$

$$k = \frac{\partial S}{\partial z} \tag{2.2.3}$$

With these assumptions, equation (2.1.1) can be used to derive a relationship between ω and k, as well as an equation for the amplitude. This relation holds even though ω and k are now allowed to be functions of time and space, so that we don't have a wave decomposition in the Fourier sense.

2.3 Phase relationship

Taking (2.2.1) into (2.1.1) produces a leading order balance that yields

$$\omega' = \frac{\mathbf{k} \cdot \mathbf{v}_D}{1 - \Psi} \tag{2.3.1}$$

and

$$\omega = \omega' - \mathbf{k} \cdot \mathbf{v}_i \tag{2.3.2}$$

with

$$\Psi = \Psi_0 \left(\frac{k^2}{k^2} - \frac{k^2 \Omega_i^2}{k^2 \nu_i^2} \right) \tag{2.3.3}$$

Here, ω' is the frequency determining the growth of the waves, which depends on the relative electron-ion drift $\mathbf{v}_D$. On the other hand, ω is the time derivative of the phase S and has to take into account the ion drift itself too. Therefore, ω / k is the phase speed in the neutral frame of reference, and ω' / k is the phase speed in the ion frame of reference.

Equations (2.3.1) and (2.3.2) show that the instantaneous frequency is a function of altitude through the variations in $\mathbf{v}_D$ and Ψ. Within the new theoretical framework, k is also no longer a free parameter. Instead, there is a connection between ω and k as can be seen by taking the mixed derivatives of the phase and equation (2.2.2):

$$\frac{\partial k}{\partial t} = -\frac{\partial \omega}{\partial z} \tag{2.3.4}$$

Because of this, a frequency that varies with z must necessarily imply a time varying $k_\parallel$, and thus an aspect angle that changes with time.

2.4 Amplitude Equation

The first order terms in equation (2.1.1) lead to

$$\frac{\partial \ln A}{\partial t} + v_g \frac{\partial \ln A}{\partial z} = \gamma_{FB} - v_g \left[\frac{1}{2k} \frac{\partial k}{\partial z} - \frac{1}{1-\Psi} \frac{\partial \Psi}{\partial z} - \frac{1}{\mathbf{k} \cdot \mathbf{v}_D} \frac{\partial \mathbf{k} \cdot \mathbf{v}_D}{\partial z} \right] \tag{2.4.1}$$

which can be written as

$$\frac{D \ln A}{Dt} = \gamma_{FB} - \frac{v_g}{2} \frac{\partial}{\partial z} \left[\ln k^2 - 2\left(\ln \mathbf{k} \cdot \mathbf{v}_D - \ln 1 - \Psi \right) \right] \tag{2.4.2}$$

or

$$\frac{D \ln A}{Dt} = \gamma_{FB} - \frac{v_g}{2} \frac{\partial}{\partial z} \left[\ln k^2 \omega'^2 \right] \tag{2.4.3}$$

where

$$\gamma_{FB} = \frac{(\omega'^2 - k^2 v_i^2)\Psi}{(1-\Psi)\nu_i} \tag{2.4.4}$$

is the standard Farley-Buneman growth rate from equation (1.6.19) and D/Dt is the convective derivative.

Also, v_g is the parallel group velocity and is determined by

$$v_g = \frac{\mathbf{k} \cdot \mathbf{v}_D}{(1-\Psi)^2} \Psi_0 \frac{2k}{k^2} \frac{\Omega_e^2}{\nu_e^2} \tag{2.4.5}$$

It really is a group velocity as can be verified by taking $\partial\omega/\partial k$.

Finally, for conciseness, we will write equation (2.4.1) in the form

$$\frac{D \ln A}{Dt} = \gamma_{eff} \tag{2.4.6}$$

with γ_{eff} being the effective growth rate representing all terms on the right hand side of equation (2.4.1)

2.5 Conservation of wave action

The presence of the convective derivative in (2.4.6) suggests that this equation is the result of a conservation principle, which in this case is not simple conservation of wave energy but rather conservation of wave action. This principle, described for example by *Bretherton and Garret* [1969], is an approximation and true only if the frequency changes slowly enough in time and space. It can be expressed as

$$\frac{\partial}{\partial t}\left(\frac{U_k}{\omega'}\right) - \nabla \cdot \left(\frac{\mathbf{v}_g U_k}{\omega'}\right) = S \tag{2.5.1}$$

where U_k is the energy of a wave with wave number k and S is a term that we have added to account for local sinks and sources of free energy. With this term it is not so much conservation of wave action but rather the balance of wave action that matters for the waves.

To determine an equation for the amplitude from (2.5.1), we need to know how energy and amplitude are related. The energy in the waves is the sum of kinetic energy of the electrons and ions as well as electrostatic potential energy. Because of their small mass, the electrons' contribution to the kinetic energy can be neglected, so that we have [from *St.-Maurice et al.*, work in progress]

$$U_k \approx \frac{1}{2} n_0 m_i \, \delta \mathbf{v}_k^{i\,2} - \frac{\delta E_k^{\,2}}{8\pi} \tag{2.5.2}$$

For Farley-Buneman waves, equation (1.5.4) shows how the ion velocity fluctuations are related to the electric field, and we have

$$\delta \mathbf{v}_k^i = \frac{\Omega_i}{\nu_i} \frac{\delta E_k}{B} \tag{2.5.3}$$

From equation (1.5.11) we see that

$$\frac{\delta n}{n_0} = \frac{\Omega_i}{\nu_i} \left(1 - \Psi\right) \frac{\delta E}{E_0} \tag{2.5.4}$$

or

$$\frac{\delta n}{n_0} = \frac{\Omega_i}{\nu_i} \frac{1-\Psi}{E_0/B} \frac{dE_k}{B} \tag{2.5.5}$$

With equation (1.5.16) for the phase speed $V = \omega'/k$, we get

$$\frac{\delta E_k}{B} = \frac{\omega'}{k} \frac{\delta n}{n_0} \frac{\nu_i}{\Omega_i} \tag{2.5.6}$$

which means we can write the peak kinetic energy, equal to the total wave energy, in the form

$$U_k \approx \frac{1}{2} n_0 m_i \left| \frac{\delta n}{n_0} \right|^2 \frac{\omega'^2}{k^2} \tag{2.5.7}$$

Using this expression in equation (2.5.1), it can be shown that the amplitude equation from conservation of wave action becomes

$$\frac{\partial \ln A}{\partial t} + v_g \frac{\partial \ln A}{\partial z} = \gamma_{FB} - \nu_i \left[\frac{1}{2k} \frac{\partial k}{\partial z} - \frac{1}{1-\Psi} \frac{\partial \Psi}{\partial z} - \frac{2-\Psi}{2\mathbf{k}\cdot\mathbf{v}_D} \frac{\partial \mathbf{k}\cdot\mathbf{v}_D}{\partial z} - \frac{\partial \ln n_0}{\partial z} \right] \tag{2.5.8}$$

This equation is very similar to the one derived from the multi-scaling expansion of the differential equation (2.1.1), i.e. (2.4.1). A small difference is the third term in the brackets, which is larger by a factor of $(2-\Psi)/2$. This is not significant though, because waves will only grow when Ψ is very small, and a large Ψ makes ω' too small to have growth. The other difference is the last term in (2.5.8), but it turns out that it is small enough to be neglected too.

The conclusion from this is that convective growth and decay can be seen as results from the conservation of wave action, or more to the point, as the balance of wave action when spontaneous Farley-Buneman growth terms are included.

Chapter 3

NUMERICAL SOLUTION

3.1 Summary of the problem

The important result from chapter 2 is that the system can be described by a set of coupled partial differential equations. To get a solution, we first need to determine k as a function of time and space. We can then calculate all the other parameters, and finally solve the amplitude equation.

The set of equations we have to solve is this:

$$\frac{\partial k}{\partial z} = -\frac{\partial \omega}{\partial t} \tag{3.1.1a}$$

$$\omega = \frac{\mathbf{k} \cdot \mathbf{v}_D}{1 - \Psi} - \mathbf{k} \cdot \mathbf{v}, \tag{3.1.1b}$$

$$\frac{D \ln A}{Dt} = \gamma_{eff} \tag{3.1.1c}$$

All other properties can be calculated from the solution to these equations.

The first two equations can be solved independently from the amplitude equation because neither depends on the amplitude, and a numerical solution can easily be obtained by the method of finite differences. In fact, when written as an equation for

k_x / k and ω / k, i.e. the aspect angle and phase speed. (3.1.1a) does not even depend on the wavelength, but *only* on the background properties, because all the terms present in equations (3.1.1a) and (3.1.1b) are only in terms of either k_x / k or ω / k.

From this we can see that the aspect angle can be determined independently and is in fact the first property we have to calculate. Then with the knowledge of $k_x(z,t)$ and $\omega(z,t)$ we can solve for the amplitude A.

3.2 Finite Differences

The first attempt to solve for the amplitude was to use the method of finite differences. It turns out to be easier to solve for $\ln A$ instead of the amplitude itself, and we have to use regular partial derivatives instead of the convective derivative in equation (3.1.1c). Then, the value of A after a small time step Δt and with a spatial step size h is given by

$$\frac{\ln A(z, t-\Delta t) - \ln A(z,t)}{\Delta t} = \alpha_{eff}(z,t) - c_g(z,t)\frac{\ln A(z-h,t) - \ln A(z-h,t)}{2h} \tag{3.2.1}$$

Here, the term $(\ln A(z-h,t) - \ln A(z-h,t))/(2h)$ is an approximation for $\partial \ln A/\partial z$. This is more accurate than the more obvious $(\ln A(z,t) - \ln A(z-h,t))/h$, but has the disadvantage that it introduces an additional boundary conditions for the amplitude, so that we have to supply a boundary condition at both the lower and upper limits of integration. While this can be worked around by choosing a good boundary condition, the other problem is a large gradient in the z direction.

At this gradient, the above approximation for $\partial \ln A/\partial z$ is no longer accurate enough, and higher order terms would have to be included for sufficient accuracy, so that the solution is very sensitive to gradients in the z direction.

However, these are inevitable because of the evolution of k which forces a convergence of rays. The resulting amplitude from solving (3.2.1) is unreasonably large. In the vicinity of the gradient, it would grow by a reasonable factor of 10 or 100, but at the gradient itself, amplitudes could reach factors of 10^{50} or more. This is impossible because, for the example shown in figure 3.1, the maximum growth rate is 41 s^{-1}, and even if the wave was growing at that rate all the time, it couldn't possibly reach an amplitude larger than $e^{41} \approx 6.4 \times 10^{17}$ after a second has passed.

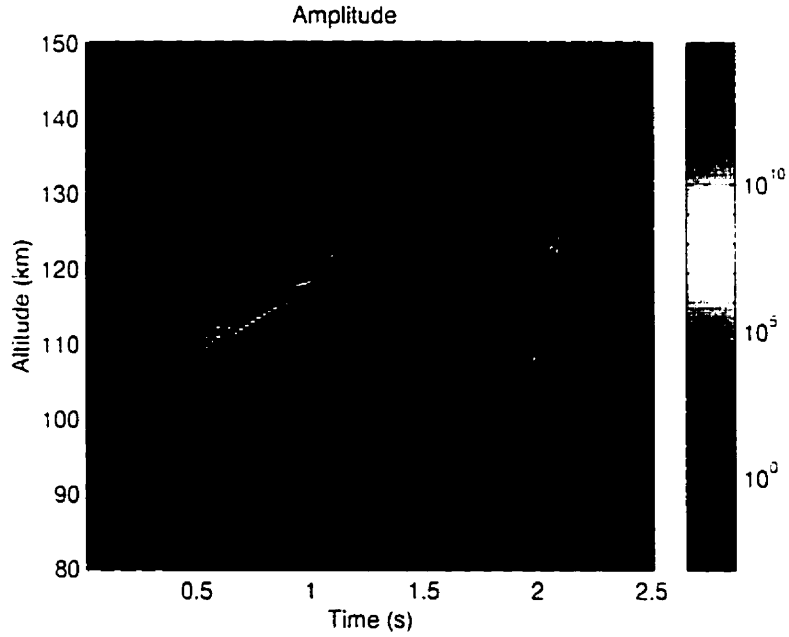

Figure 3.1: Wave amplitude from a finite difference calculation

Another side effect from this algorithm and the large amplitudes is that each of the grid points in question will in turn seed a new wave, leading to "fingers" trailing each peak in the amplitude, as can be seen in figure 3.1. Therefore these amplitudes are clearly numerical instabilities and the algorithm is unsuitable to solve this differential equation.

The reason for this is that (3.1.1c) turns out to be a stiff equation which is very

hard to solve using the finite difference method. Decreasing the step sizes helped somewhat, but the numerical instabilities were still present, and the incurred penalty of a much greater cost of computation along with possibly increased numerical error didn't make it worthwhile. A different approach to solving the problem is clearly necessary, one which takes into account both the stiffness of (3.1.1c) as well as the convergence leading to gradients in the z direction.

3.3 Method of Characteristics or Ray tracing

The method of characteristics does a much better job of solving the amplitude equation. This method is often used to solve fluid equations involving time derivatives and gradients, for example Euler's equation from incompressible, frictionless flow:

$$\rho\left(\mathbf{v}\cdot\nabla-\frac{\partial}{\partial t}\right)\mathbf{v}=\mathbf{F}-\nabla p \tag{3.3.1}$$

Here, the term in parentheses is again the convective derivative, and can be abbreviated as D/Dt. It is the time derivative when following the motion of the fluid.

The same analysis can be applied to our amplitude equation, which also involves a convective derivative. Looking again at equation (3.1.1c), we have

$$\frac{D\ln A}{Dt}=\gamma_{eff} \tag{3.3.2}$$

where

$$\frac{D}{Dt}=\frac{\partial}{\partial t}-v_g\frac{\partial}{\partial z} \tag{3.3.3}$$

Solving this equation with the method of characteristics amounts to following the paths of "rays", which are given by $z_n(t)$ such that

$$\frac{dz_n(t)}{dt}=v_g\left(z_n(t),t\right) \tag{3.3.4}$$

where n is the number of the ray. Then we have

$$\frac{d \ln A(z_n(t), t)}{dt} = \gamma_{eff}(z_n(t), t) \tag{3.3.5}$$

Equations (3.3.4) and (3.3.5) can be solved independently, and both are simple first-order ordinary differential equations. Equation (3.3.4) will give the path of the rays, the altitude as a function of time, and (3.3.5) gives the amplitude evolution along that particular ray path.

This method is raytracing in this case even though the equations seem to involve only the z and t axes. The reason is that the waves also propagate in the x direction, which is perpendicular to B, with a constant group velocity of $v_{g\perp} = E \times B$. Therefore,

$$x(t) = v_{g\perp} t = \frac{E}{B} t \tag{3.3.6}$$

so that

$$\frac{dz}{dx} = \frac{dz}{dt}\left(\frac{dx}{dt}\right)^{-1} = \frac{v_g}{v_{g\perp}} \tag{3.3.7}$$

which means that the rays propagate in the direction given by

$$\tan\alpha = \frac{dz}{dx} = \frac{v_g}{v_{g\perp}} \tag{3.3.8}$$

i.e. the ray path is in the direction of $\mathbf{v}_g$ itself. From this we can see that taking the ray path to be $z(t)$ or $z(x)$ is equivalent.

Now we can see that this way of solving the amplitude equation is guaranteed to work, and both the ray altitudes and the amplitude following the ray have stable numerical solutions. The reason for this is that now they are just two ordinary differential equations replacing the partial differential equation in space and time.

The convergence that caused problems for the finite difference calculation is now accounted for by the ray paths, and the stiffness is no longer a problem because we can

solve for each ray independently of the other rays. However, there is one additional correction that has to be considered. Where the rays are converging, the energy is concentrated in a smaller amount of space. The amplitude equation for the rays does not take this effect into account. To get the wave amplitude from the set of rays, we must therefore correct the ray amplitude by a factor related to the ray density. A higher ray density means the amplitude has to be increased and vice versa. We can determine the ray density from the average distance to the two adjacent rays:

$$\rho_n = \frac{2z_0}{z_{n-1}(t) - z_{n-1}(t)} \tag{3.3.9}$$

where n is the ray number and z_0 is the initial ray spacing to normalize the density. For the first and last ray, this equation is of course modified appropriately. Then the correction factor can be written as

$$A^2_{n,corrected} = A^2_n \rho_n \tag{3.3.10}$$

We correct A^2 instead of A because the energy is proportional to A^2. The correction factor turns out to be to the order of $\rho \approx 40$–50 in the region where the amplitude is largest, or an amplitude correction of a factor of about 7.

Once we have the corrected ray amplitude, we use a linear interpolation technique to get a regularly spaced grid of the wave amplitude which allows for easier plotting.

3.4 Initial Conditions

There are two initial conditions that have to be specified, one on the amplitude and one on k. However, the only physical condition we have is the physical shape of the wave packet, given by $A\exp(iS)$. This means that we have to find amplitude A and phase S such that they give the shape we want our wave train to have. The initial

conditions should also satisfy the assumptions made in the derivation, namely that

$$\left|\frac{\partial \ln A}{\partial z}\right| \ll k \tag{3.4.1a}$$

$$\left|\frac{\partial \ln A}{\partial t}\right| \ll \omega' \tag{3.4.1b}$$

The easiest way to satisfy this is to have the amplitude be equal to 1 at all altitudes so that $\partial \ln A / \partial z = 0$, and define S in a such way that the real part of $A\exp(iS)$ describes the desired density fluctuation. The amplitude will be proportional to the initial value of A, so choosing $A = 1$ is as good as any other value.

The initial shape we chose was a Gaussian distribution of width H centered at a particular altitude z_0 to model a local enhancement in plasma density, much like the clump discussed in chapter 1. Now we can derive the initial condition for k as follows:

$$\Re\left[A\exp(iS)\right] = \exp\left[-\left(\frac{z - z_0}{H}\right)^2\right] \tag{3.4.2}$$

$$\cos S = \exp\left[-\left(\frac{z - z_0}{H}\right)^2\right] \tag{3.4.3}$$

$$k(z, t = 0) = \frac{\partial S}{\partial z} = \frac{\partial \cos S}{\partial z}\left(\frac{\partial \cos S}{\partial S}\right)^{-1} \tag{3.4.4}$$

and finally

$$k = \frac{2(z - z_0)\cos S}{H^2}\left(\pm\left[1 - \cos^2 S\right]^{1/2}\right)^{-1} \tag{3.4.5}$$

with a maximum k at $z = z_0$ of

$$k_{max} = \lim_{z \to z_0} k = \pm\frac{\sqrt{2}}{H} \tag{3.4.6}$$

The ambiguity in the sign is introduced by writing $\sin S = \pm(1 - \cos^2 S)^{1/2}$ for easier manipulation of the equations. It is not important however, because $\cos S$ has the same value no matter which sign we choose. In our case, we have chosen

the frequency to be positive, so that k will evolve towards more negative values, and so we use the negative sign in equation (3.4.5). The reason for this is that ω is increasing monotonically with altitude, therefore equation (3.1.1a) predicts a monotonically decreasing k.

For the case discussed in chapter 4, with $H = 5$ km, $z_0 = 95$ km and $\lambda = 12$ m, we get $k_{max} = \pm 2.828 \times 10^{-4}$ m^{-1}, which corresponds to a maximum aspect angle of ± 0.0310 degrees. The initial k value along with the phase and cos S in this particular case is shown in figure 3.2.

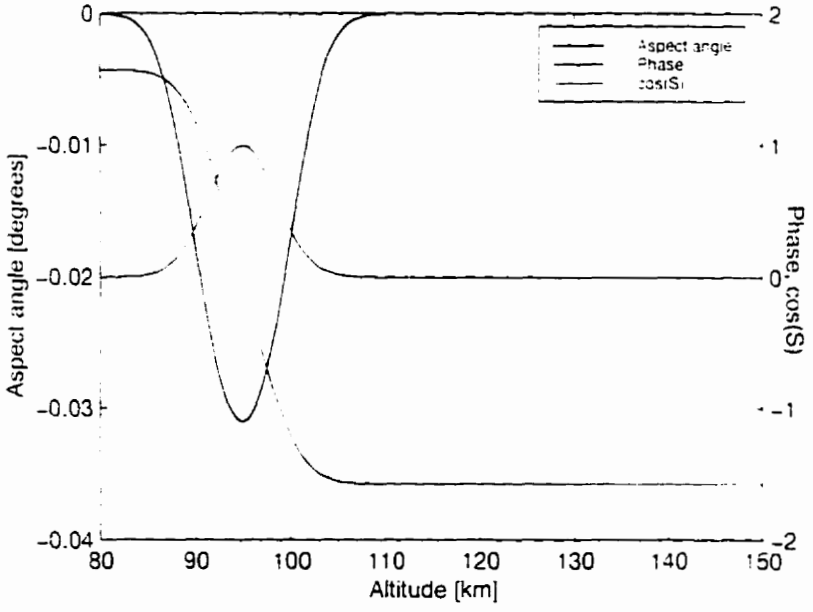

Figure 3.2: Initial aspect angle and phase for $H = 5$ km, $z_0 = 95$ km and $\lambda = 12$ m

3.5 Boundary Conditions

Using the method of characteristics, no boundary conditions are needed for the amplitude equation because it is solved by two ordinary differential equations which only

need initial conditions.

The solution to equation (3.1.1a) for k does need one boundary condition, however. We chose the boundary to be at a height of 150 km, where the relative drift between electrons and ions v_D is so small that Farley-Buneman instabilities cannot grow according to (1.6.23) and wave amplitudes are therefore insignificant.

At this altitude, the phase speed ω / k as given by the solution to equation (3.1.1b) is approximately equal to the $\mathbf{E} \times \mathbf{B}$ drift and uniform. Thus, ω is uniform and therefore

$$\frac{\partial k}{\partial t} = -\frac{\partial \omega}{\partial z} = 0 \tag{3.5.1}$$

So, the boundary condition is that at 150 km, k does not change in time.

$$k\ (150\ \text{km}, t) = k\ (150\ \text{km}, 0) \tag{3.5.2}$$

3.6 Background Properties

The next important consideration is what to use for the properties of the background. These will determine both the evolution of k and thus the ray paths, as well as the growth rate for the amplitude along the path of each ray.

Our electron, ion and neutral temperature are based on the MSIS-90 model [*Hedin*, 1991], however the electron temperature has been modified to reflect the additional electron heating discovered by *Schlegel and St.-Maurice* [1981]; *St.-Maurice et al.* [1981] which is not included in the MSIS-90 model. The temperature profiles are shown in figure 3.3.

MSIS-90 has also been used to calculate neutral densities, electron-neutral and ion- neutral collision frequencies, and the relative drifts between electrons, ions and neutrals, with the results shown in figures 3.4, 3.5 and 3.6.

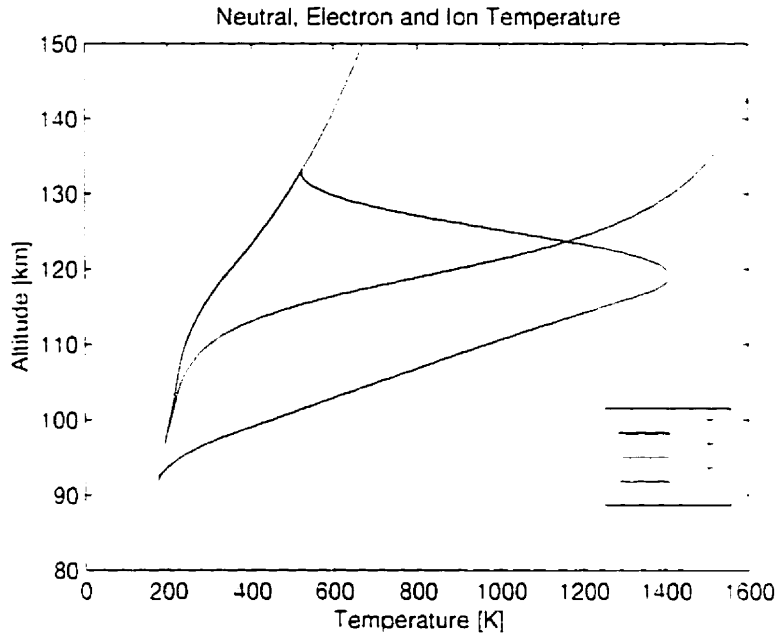

Figure 3.3: Temperature profiles for electrons, ions and the neutrals

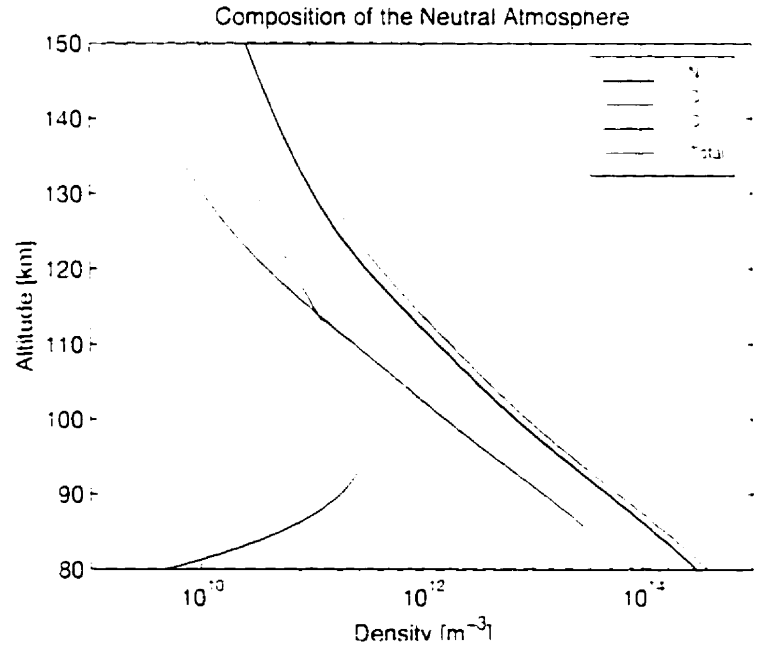

Figure 3.4: Neutral densities

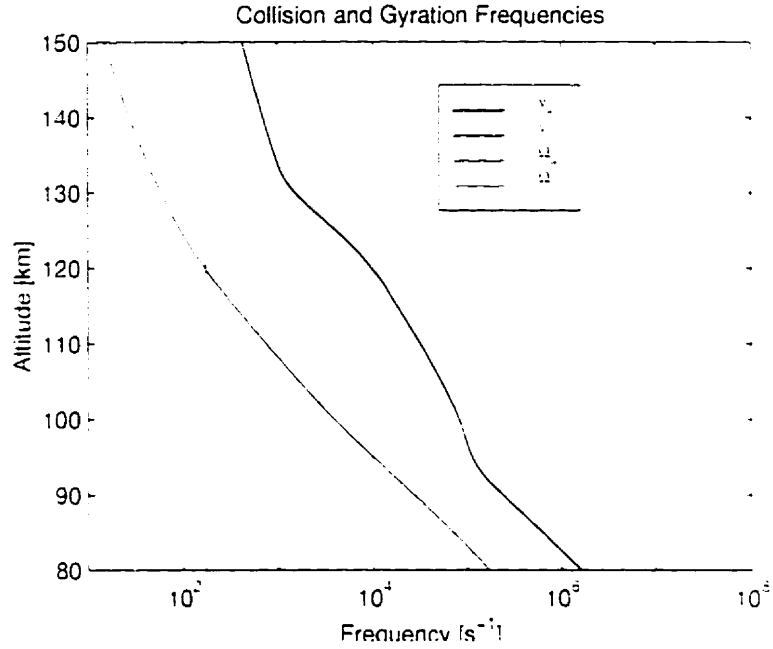

Figure 3.5: Collision and gyration frequencies for electrons and ions

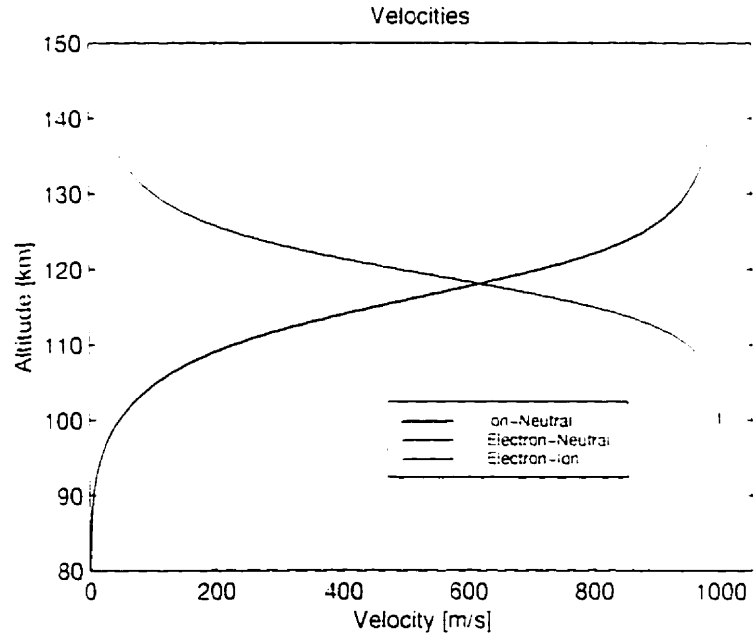

Figure 3.6: Relative velocities between the three species

For the purpose of this study, the electric field $\mathbf{E}$ and magnetic field $\mathbf{B}$ are assumed to be constant and uniform throughout the experiment.

The next chapter will then describe the results we got from the programs listed in appendix A, which solve the differential equations using the methods described in this chapter.

Chapter 4

RESULTS

In this chapter we will present the results from the study. We will start with a detailed analysis of a particular case, and then compare the results to observations made with radars.

We chose the wavelength to be 12 m, corresponding to a radar frequency of 12.5 MHz, because it is a common frequency used by the SuperDARN chain of radars (see *Greenwald et al.*, 1978, 1985). Also, the large growth rates associated with much shorter wavelengths would make the waves become non-linear before they have time to move through the ionosphere, so that this linear model would not apply anymore.

We also took the electron $\mathbf{E} \times \mathbf{B}$ drift to be 1000 m/s in this case, corresponding to an electric field of 54 mV/m. This is a relatively strong field but not too unusual, and weaker electric fields do not give as much information about the phase speed for example. Also, these choices give a growth rate which is balanced between not growing enough to make a difference and growing so much that the basic assumption that the amplitude can be separated from the phase doesn't hold anymore. If the waves grow too fast, the derivatives of the amplitude become comparable to the derivatives of the phase, and the WKB method described in section 2.2 is no longer valid.

4.1 Aspect Angle Evolution

The aspect angle is the variable which controls the ray paths and thus convective effects as well as the growth rate through non-local effects. It must therefore be the starting point in the study, and can fortunately be determined completely separately.

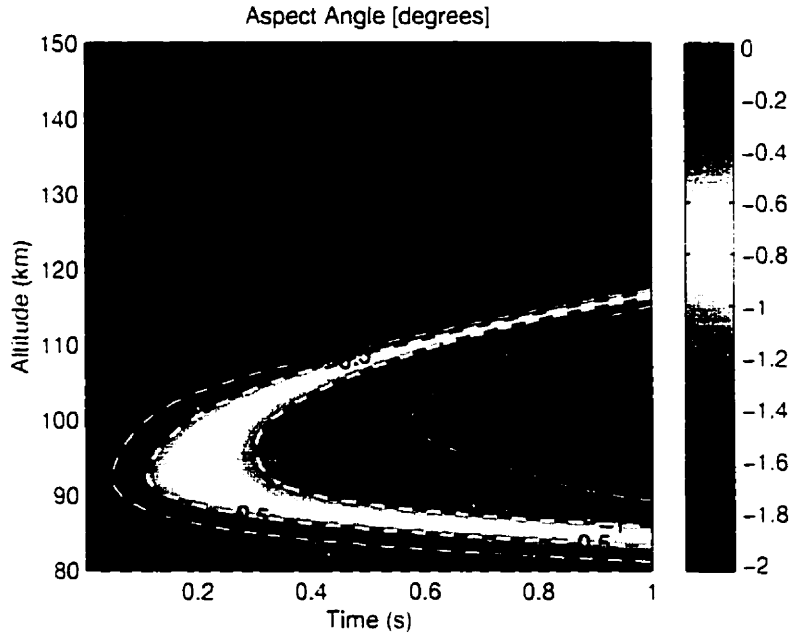

Figure 4.1: Evolution of the aspect angle as a function of altitude and time. Contours are added for emphasis.

Figure 4.1 shows the evolution of the aspect angle. The initial value comes from the use of a finite initial pulse, as described in equation (3.4.5). The magnitude of the peak initial aspect angle of -0.031 degrees at 95 km is obviously much less than the evolved values. The key thing to note here is that k is changing monotonically. In this study it is decreasing but that is because we chose the frequency to be positive. Negative frequencies imply the opposite sign in k as well, even though initially, it is possible for both to have the same sign. However, the evolution will always be such that a wave travels to higher altitudes, because the group velocity keeps the sign

when we switch both k and ω to the opposite sign.

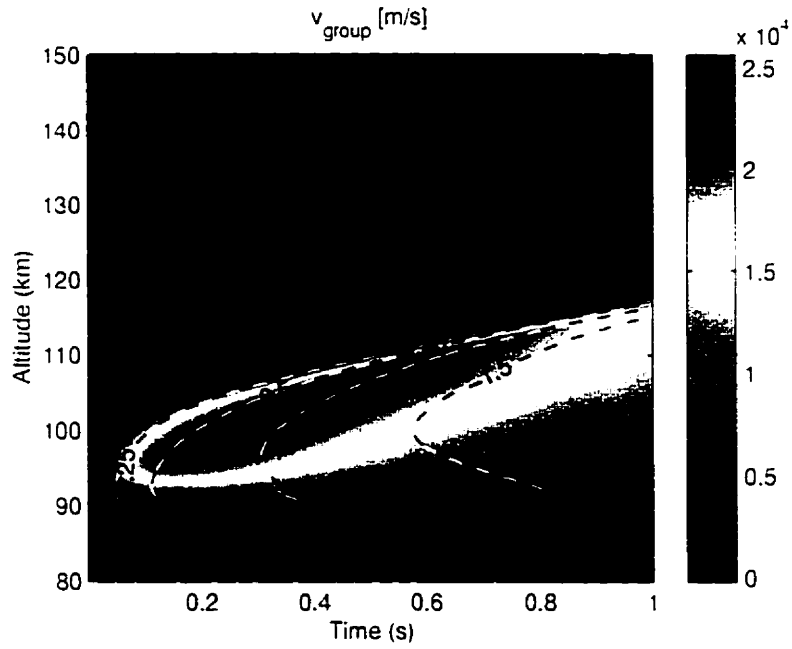

Figure 4.2: Group Velocity as function of altitude and time. Contours of the aspect angle are superimposed on the plot.

The region of interest is the part of the evolution where parallel electric fields have developed, but are not yet strong enough to cancel growth of the waves. This is the case for aspect angles between zero and approximately one degree in magnitude. In particular, the -0.5 degree contour is most interesting because, as we will show later, it turns out that this is where the amplitudes are largest.

Directly related to the aspect angle and proportional to it is the parallel group velocity, or the ray velocity, shown in figure 4.2. It is positive everywhere as expected from the aspect angle being negative. From the group velocity we can then immediately determine the ray paths through definition (3.3.4), they are shown in figure 4.3.

The most interesting property of group velocity and the rays is the convergence,

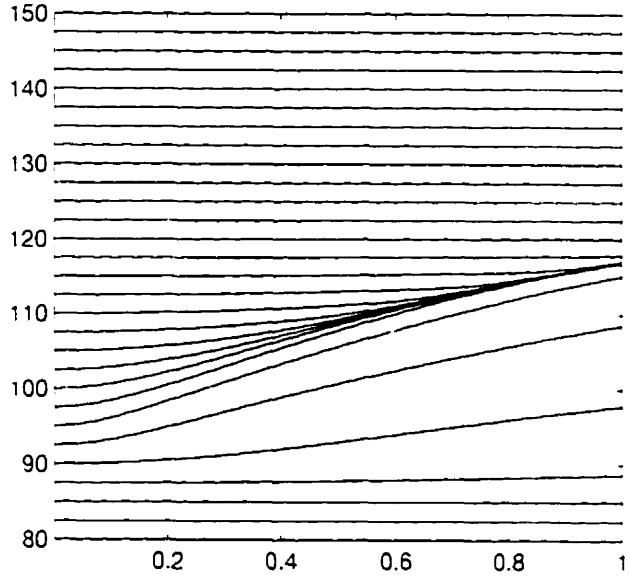

Figure 4.3: Ray Paths

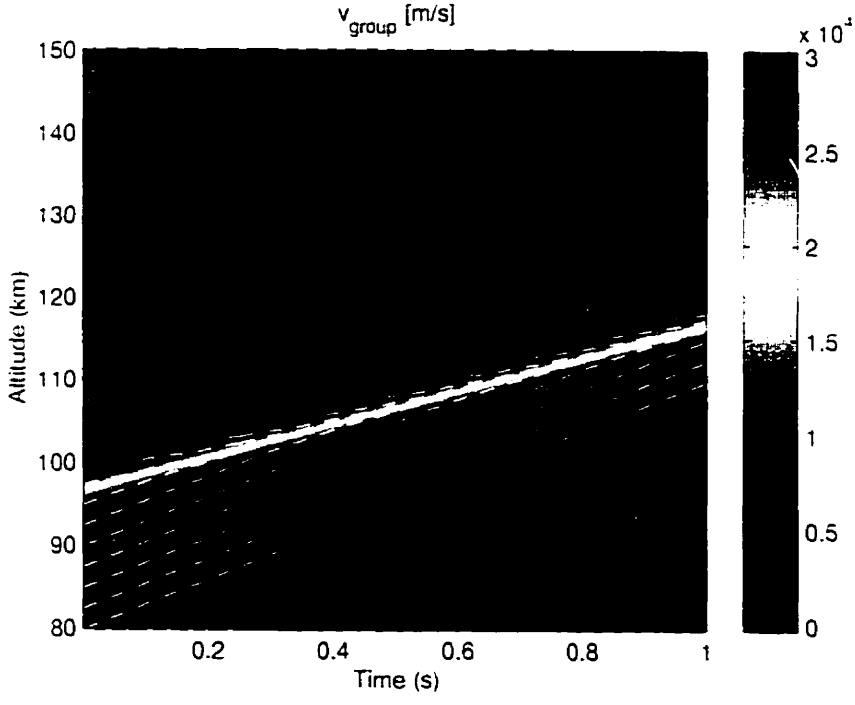

Figure 4.4: Simplified example of the group velocity for a better understanding of the convergence.

This effect occurs in regions above the peak in v_g in such a way that the rays all try to have a group velocity which matches the vertical speed at the altitude where the rays are converging. Unfortunately both this speed and the altitude of convergence are changing with time, making this process rather complicated.

To better understand this effect, consider the following simplified scenario, depicted in figure 4.4. Let the group velocity evolve in such a way that the shape of the vertical profile does not change with time, but is as a whole moving upwards with a speed of 1×10^4 m/s, which will correspond to the speed of the center of convergence. All values above this center are smaller and all values below are higher.

This means that rays that are faster than the center of convergence, i.e. they are below it, will move upwards faster and catch up with it. They cannot pass it however. On the other hand, rays above the center are slower so that they will eventually get caught because they don't move upwards fast enough. In the end, all the rays end up moving at the group velocity equal to the speed of the center of convergence, and the only place where they can have that speed is *at* that center.

In the results from our calculation, the speed of the center of convergence is changing with time, as can be seen from the changing slope in figure 4.3.

4.2 Growth Rates

There are two growth rates involved in this model. One is γ_{FB}, the local or spontaneous growth rate which is that of the standard Farley-Buneman waves without any parallel electric field or other non-local effects. Of greater importance is the effective growth rate γ_{eff} which also has non-local terms in addition to γ_{FB}. They are shown in figures 4.5 and 4.6, respectively.

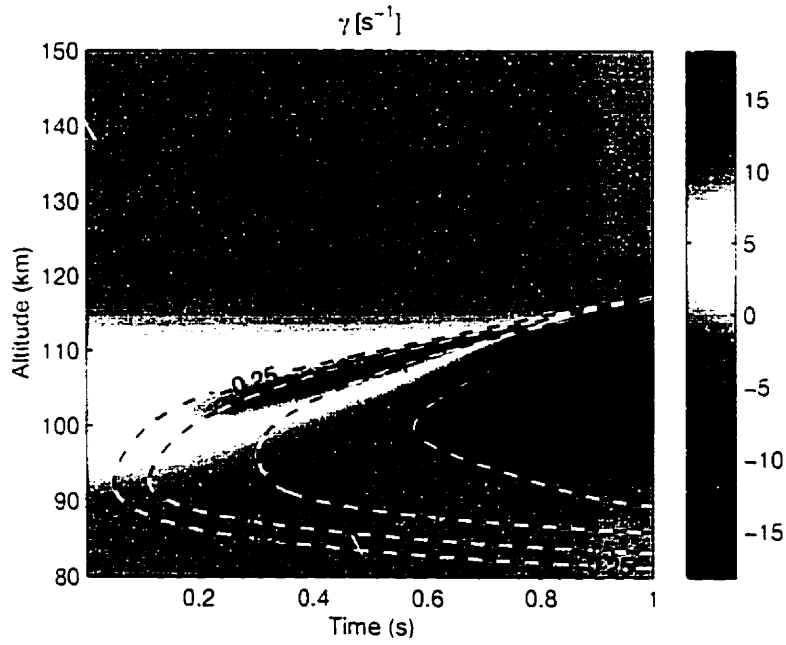

Figure 4.5: Local Farley-Buneman Growth Rate

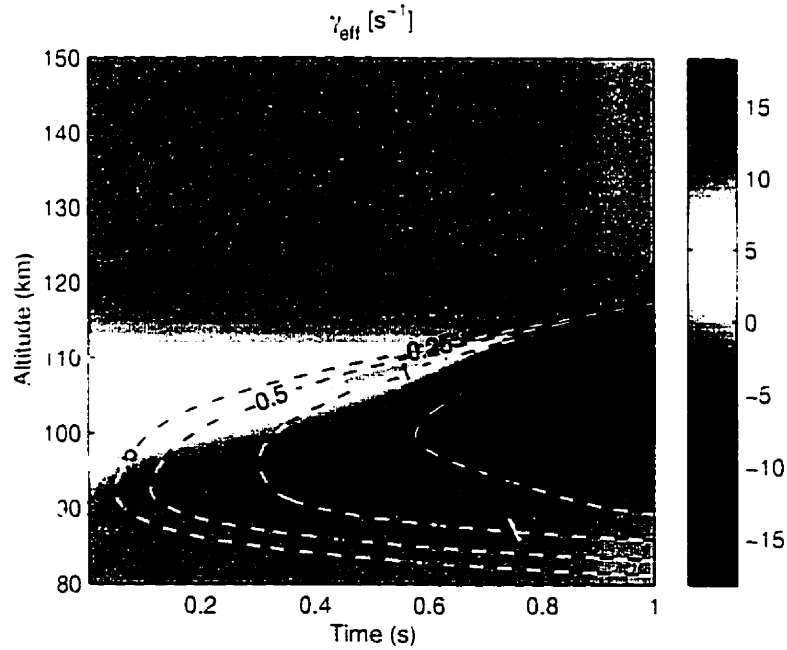

Figure 4.6: Effective Growth Rate including non-local terms.

Even though γ_{FB} might be expected to stay constant, it does in fact vary with the changing phase speed which in turn depends on Ψ through $k_\perp$ $k_\parallel$, shown in figure 4.8. At first there is an increase in growth up to a value of about $8\ s^{-1}$ but then very quickly the phase speeds get too small to sustain growth and the growth rate becomes negative.

For growth, the phase speed needs to be larger than the ion-acoustic speed, and because it depends on the relative electron-ion drift, it decreases rapidly above 120 km, where the ions start to $\mathbf{E} \times \mathbf{B}$ drift. Another factor inhibiting growth are large aspect angles of more than 0.5 degrees. For these, the electric field has a component parallel to the electric field. In this direction the electrons are very mobile and can easily short out the electric field, thereby reducing the amplitude of the wave, as can be seen in figure 4.5.

The effective growth rate on the other hand is even smaller than γ_{FB}, which shows how the convective effects and the parallel electric field work to reduce growth.

Figure 4.7 shows the phase speed relative to the neutral frame of reference, which is what ground based measurements like radars would see.

4.3 Amplitude

From the effective growth rate, we can determine the amplitude along the rays, together with the ray path as a function of height. Figures 4.9 and 4.10 show the amplitude, after the correction for the convergence, i.e. after multiplying it by the ray density as described in section 3.3. On figure 4.9 the ray paths are superimposed, nicely showing how the convergence coincides with the largest amplitudes. However, even without the correction for convergence the amplitude is still maximal in the

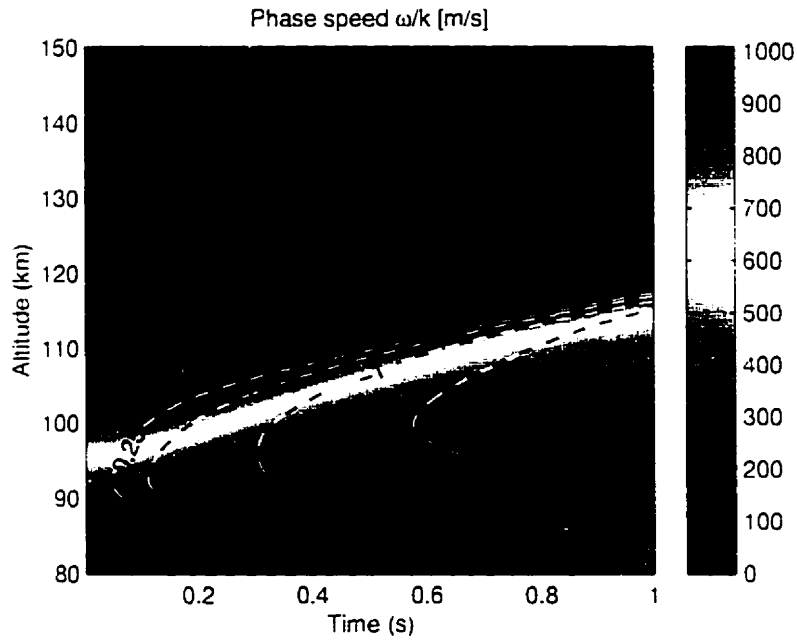

Figure 4.7: Phase Speed in the neutral frame of reference (for the propagation of the waves)

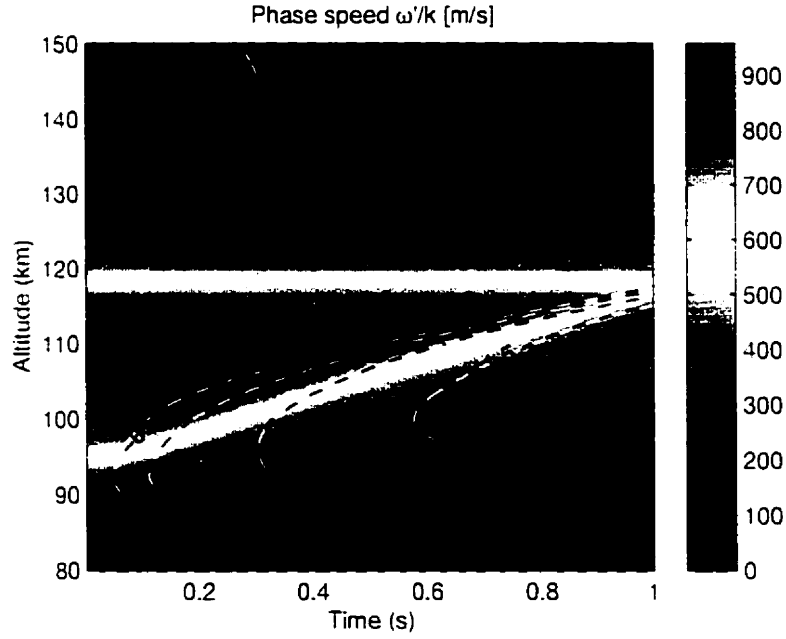

Figure 4.8: Phase Speed in the ion frame of reference (for the growth of the waves)

same region. Convergence of the rays and high growth rates are separate processes, and yet they occur in the same region.

The second figure, 4.10, shows how the largest amplitudes depend on the aspect angle. It turns out that the region with large amplitudes closely follows the -0.5 degrees contour.

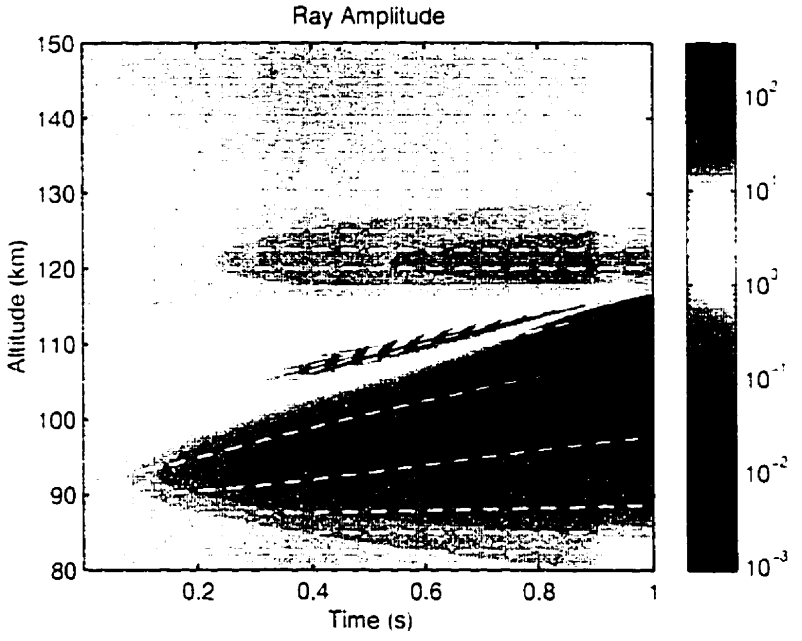

Figure 4.9: Wave Amplitude, calculated from the rays and corrected for convergence. Superimposed are the ray paths.

Both figures show very nicely that there is indeed a wave, and that it is traveling. They represent only a single wave train, the amplitude of which is distributed over a significant region of space, making it obvious why a non-local approach was necessary. Most of the growth happens in the region from 100–110 km. Above this, the electron-ion drift has decreased and the ion-acoustic speed c_s has increased so much that the growth rate becomes zero or negative.

The wave train however has gained enough amplitude before reaching this height,

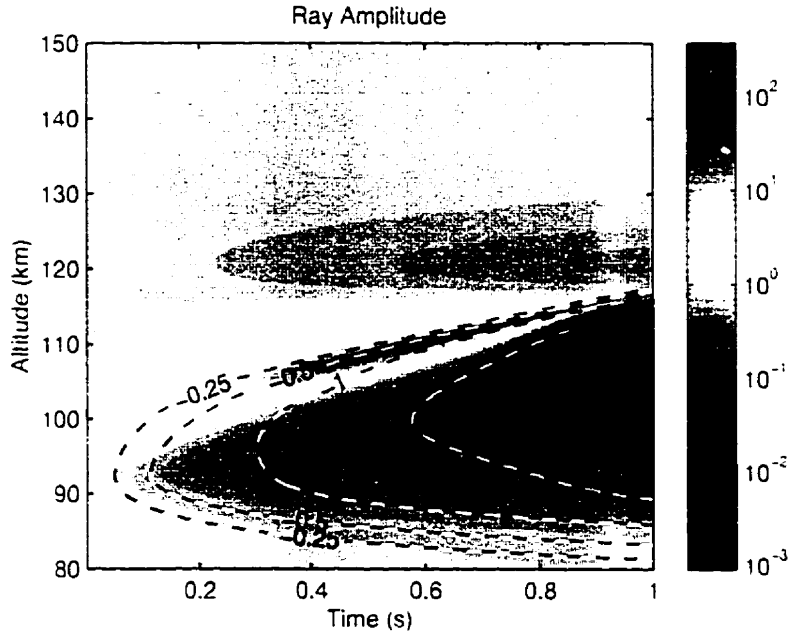

Figure 4.10: Wave Amplitude with aspect angle contours superimposed.

and continues to travel upwards for a while with decaying, but still sufficiently large, amplitude. Through this process, we can have a significant amplitude even in regions where the growth rates are too small to support it.

When trying to compare these results to observations, however, the amplitude plot is not very useful by itself, because it cannot be measured experimentally as a function of time and space. All measurements will be subject to averaging both in time and in space, and will not be able to detect a single wave train, but rather a power spectrum of the phase speed. Through finding the echo location, the aspect angle can be determined as well.

Therefore the next step will have to be to determine the amplitude of the wave train as a function of phase speed and aspect angle, and compare these results to observations.

4.4 Fourier Transforms

To get the amplitude as a function of phase speed or aspect angle, we have Fourier transformed the full solution $A\exp(iS)$. This requires determining the phase S, which can be done by integrating equations (2.2.2). The result is shown in figure 4.11. The phase plot also shows very nicely how a non-uniform frequency must necessarily lead to a vertical wave structure, expressed by the parallel wave number $k_{\parallel}$. Initially, the oscillations are in phase at all altitudes, but the difference in frequency ensures that this cannot be true at all times. Instead, the oscillators at two adjacent altitudes will be increasingly out of phase by an amount given by the non-uniformity of the frequency. At higher altitudes, the phase is changing more rapidly than at lower altitudes, and this difference in phase gives rise to a vertical structure in the wave train, described by a non-zero parallel wave number.

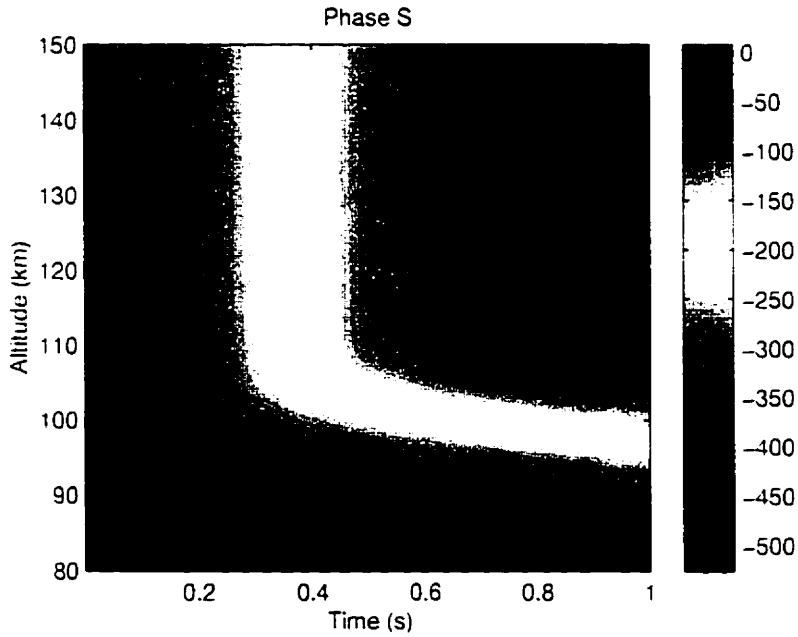

Figure 4.11: Phase of the wave

The results from taking the FFT of this solution with respect to time, space and

both are shown in figures 4.12, 4.13 and 4.16.

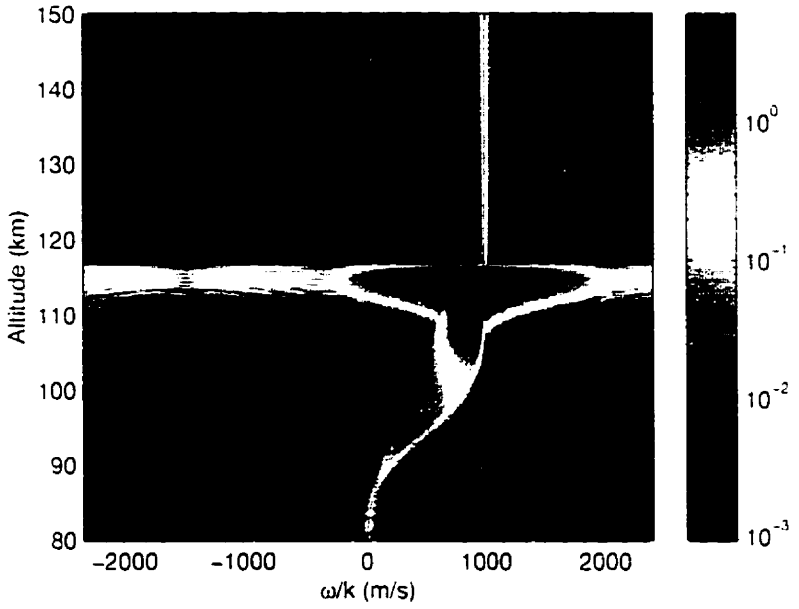

Figure 4.12: Amplitude as function of phase speed from the FFT with respect to time.

Unfortunately the FFTs turn out not to be very useful to study. The biggest problem is again the sharp gradient in the amplitude. The gradient occurs perpendicular to the ray paths and is thus unimportant for meeting the basic assumption about a slowly varying amplitude. Nonetheless, the FFT does not take ray paths into account, and therefore this gradient will affect the FFT and lead to spillover into adjacent frequencies or wave numbers. As can be seen from the plots, after about 0.6 seconds in figure 4.12 and for altitudes above 110 km in figure 4.13 this spillover becomes larger than the actual range of frequencies, making it impossible to gain any useful insight from the plots. In figures 4.14 and 4.15 we only show the actual range of phase speeds and aspect angles we see in figures 4.1 and 4.7.

Another problem is the inability to give information on how the amplitude changes with aspect angle and height, because to get the aspect angle, all heights have to be

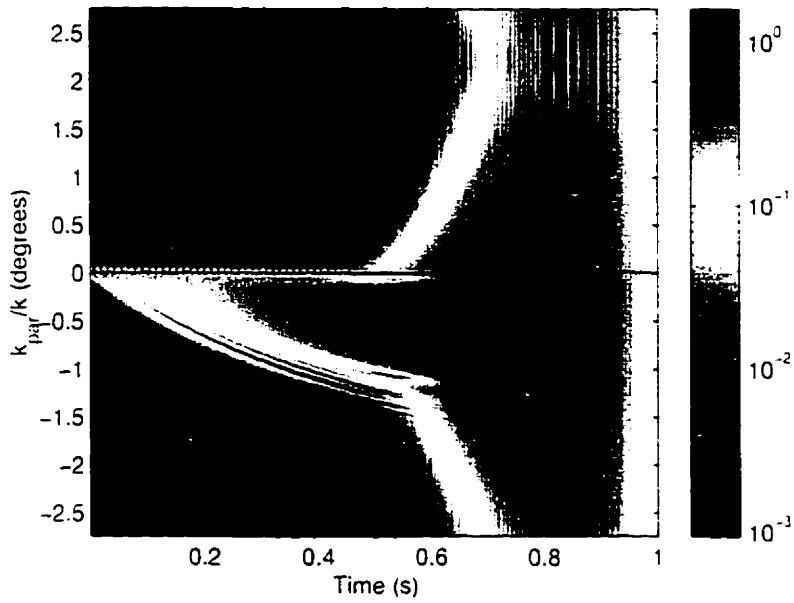

Figure 4.13: Amplitude as function of aspect angle from the FFT with respect to space.

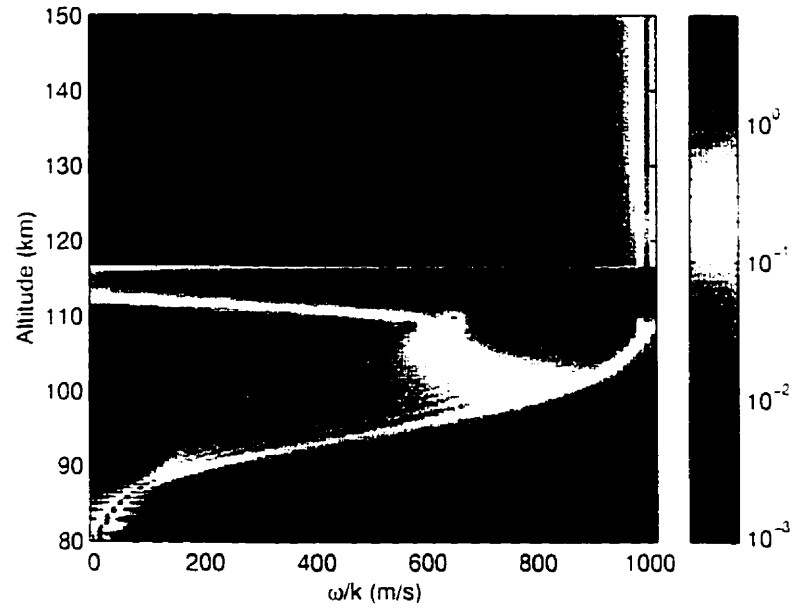

Figure 4.14: Same as figure 4.12, but only showing the range of phase speeds we have from ω k.

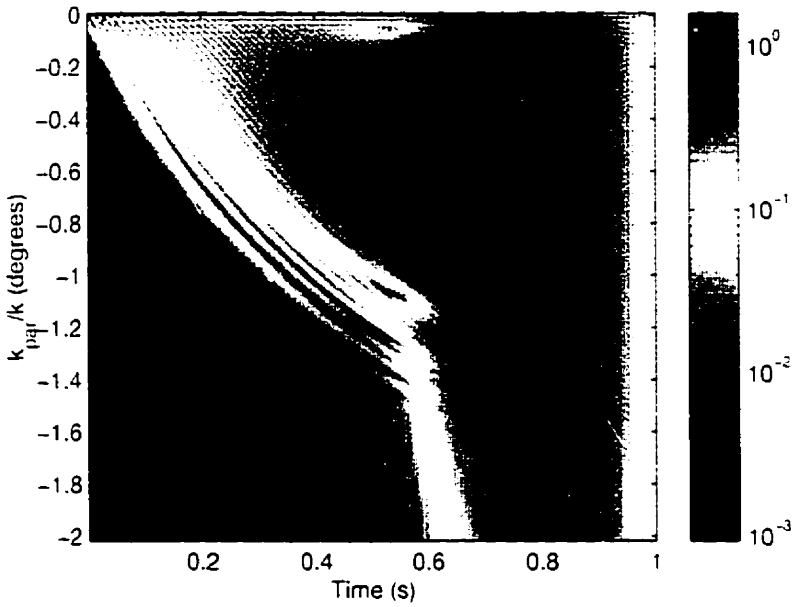

Figure 4.15: Same as figure 4.13, but only showing the range of aspect angles we have from k – k.

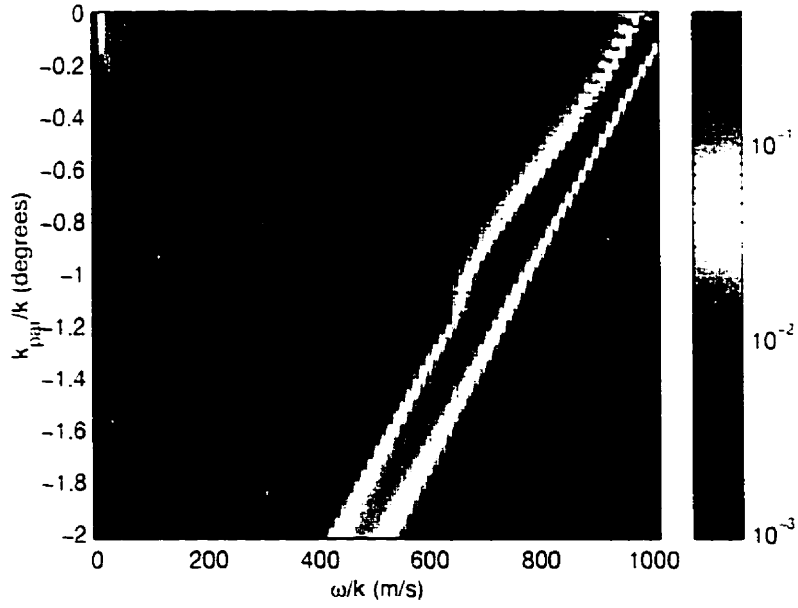

Figure 4.16: Amplitude as function of both phase speed and aspect angle from the double FFT with respect to time and space, scale is limited as in figures 4.14 and 4.15.

integrated in the Fourier transformation. One could try to circumvent this problem by having a moving window over which the transformation is done which would then give an indication on how the amplitude varies with aspect angle and height, but the resolution of the plot would have to be much better, which makes it impractical because of limited computing resources.

4.5 A Better Way

So the FFT is not much of a help in gaining insight, but maybe there is a better way? And fortunately, there is. In this setup, FFTs are in fact a large detour: first to calculate the phase from the aspect angles and phase speeds, and then applying the FFT to get back to aspect angle and phase speed.

A more direct approach is to instead look at the phase speed and aspect angle plots themselves, and find a way to combine them with the amplitude to give amplitude as a function of aspect angle and phase speed.

The basic step in this procedure is shown in figure 4.17, for the example of obtaining $A(z, k_i)$. We take a particular altitude, for example 110 km, and basically do a k -histogram of the amplitude, by going through all time steps and noting the particular amplitude for the particular k_i given at that time. The result is a function defining $A(110\text{ km}, k_i)$ with an irregular spacing between the points which is determined by the shape of $k_i(110\text{ km}, t)$. After interpolating and repeating this for all other altitudes, we can then plot $A(z, k_i)$. The same procedure can be used to replace any of the original axes z and t with either the aspect angle or the phase speed, to give all possible combinations. The results of this are shown in figures 4.18 through 4.23.

Of particular importance are the altitude plots. Figures 4.21 and 4.22 predict how

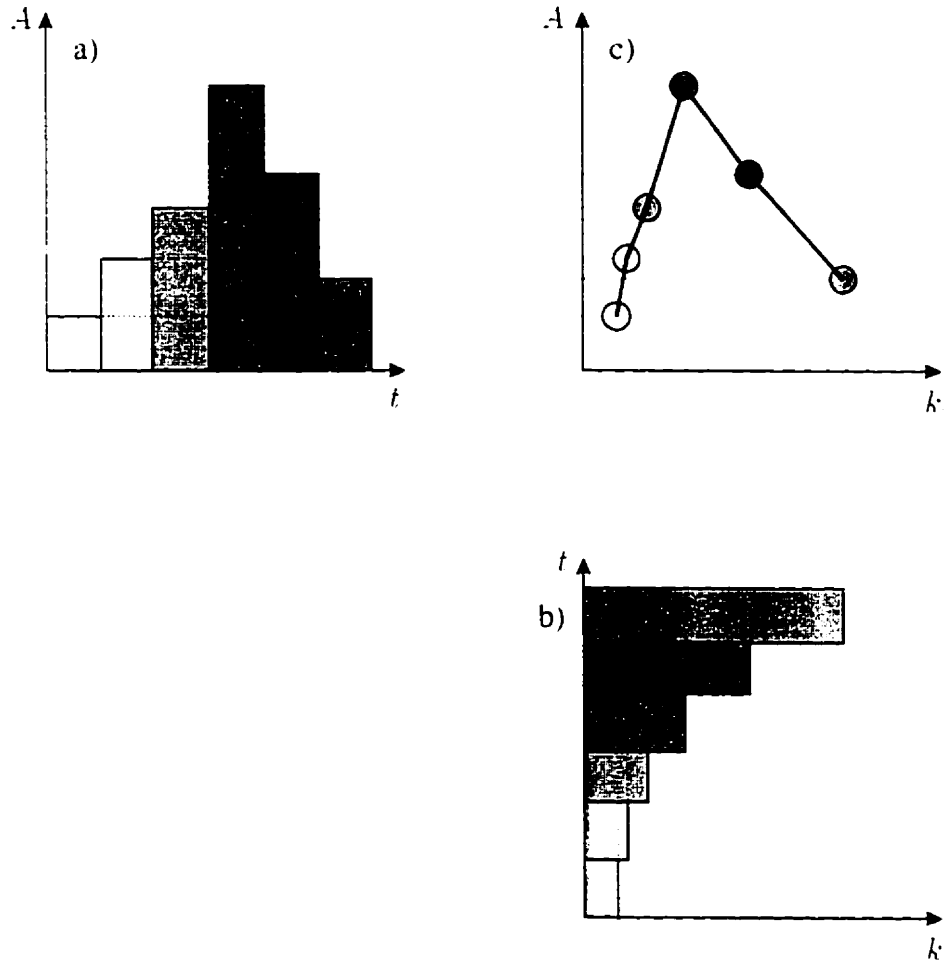

Figure 4.17: Obtaining $A(z, k)$. a) $A(z, t)$ and b) $k(z, t)$ can be combined to give c) $A(z, k)$

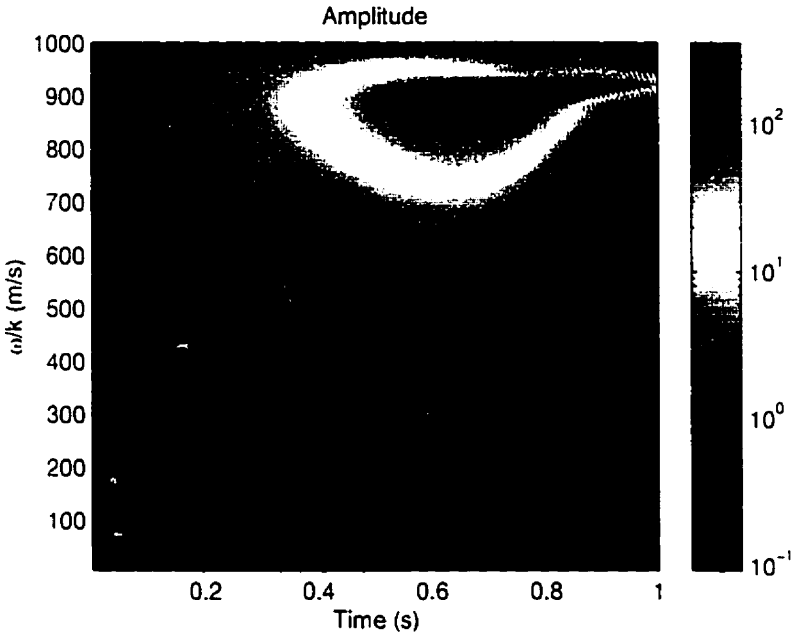

Figure 4.18: Spectrum of phase speed in time

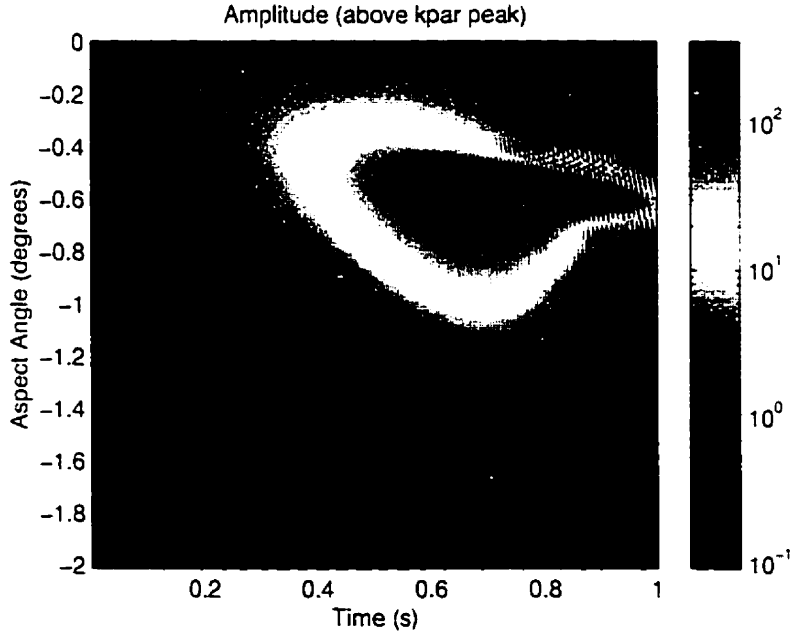

Figure 4.19: Spectrum of aspect angles in time. above the peak in $k_{\parallel}$.

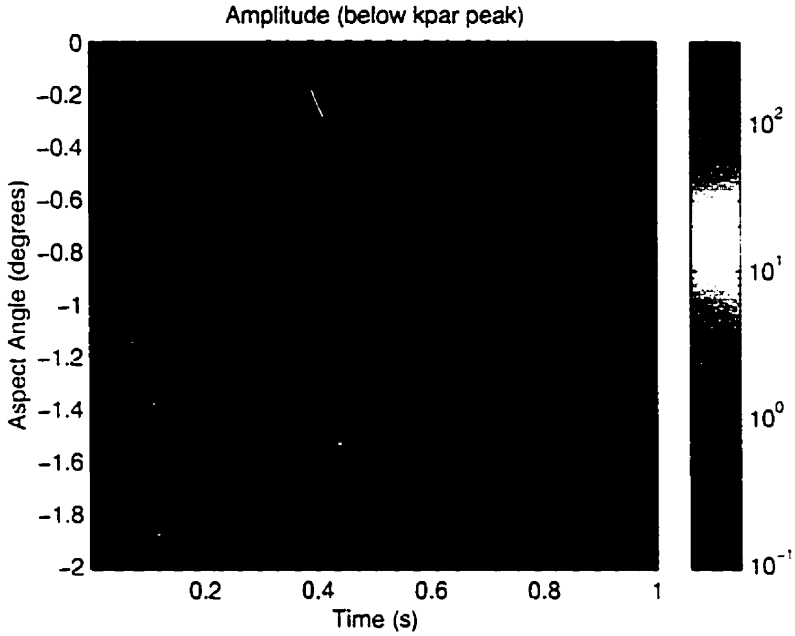

Figure 4.20: Same as figure 4.19 but below the $k_{\parallel}$ peak.

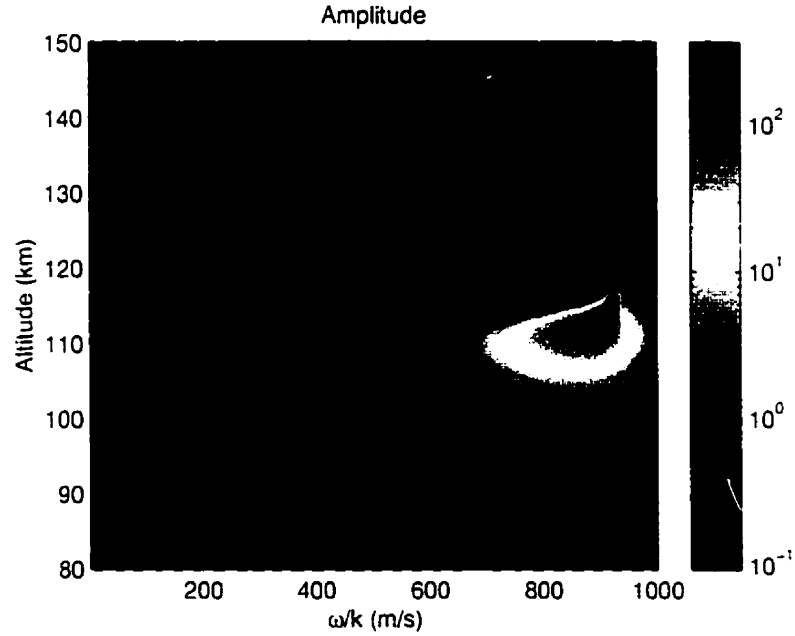

Figure 4.21: Spectrum of phase speeds and altitudes

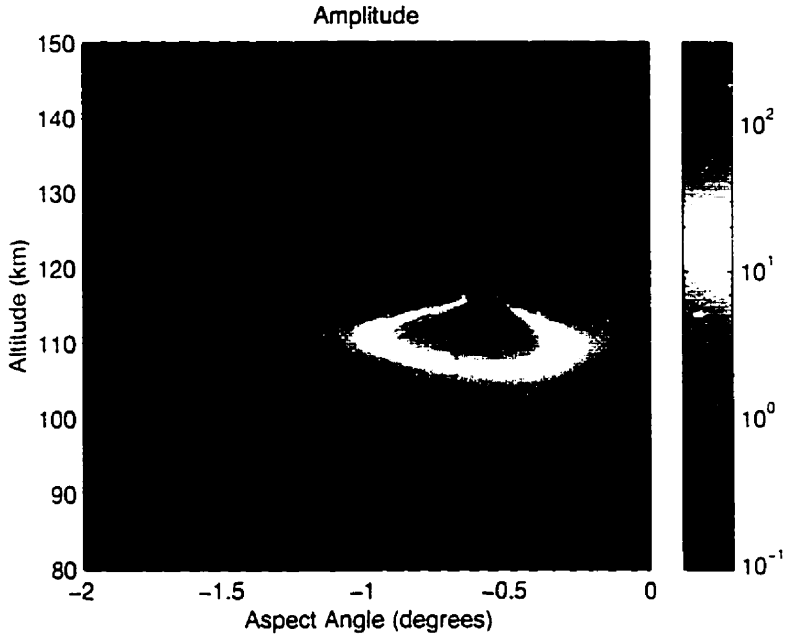

Figure 4.22: Spectrum of aspect angles and altitudes

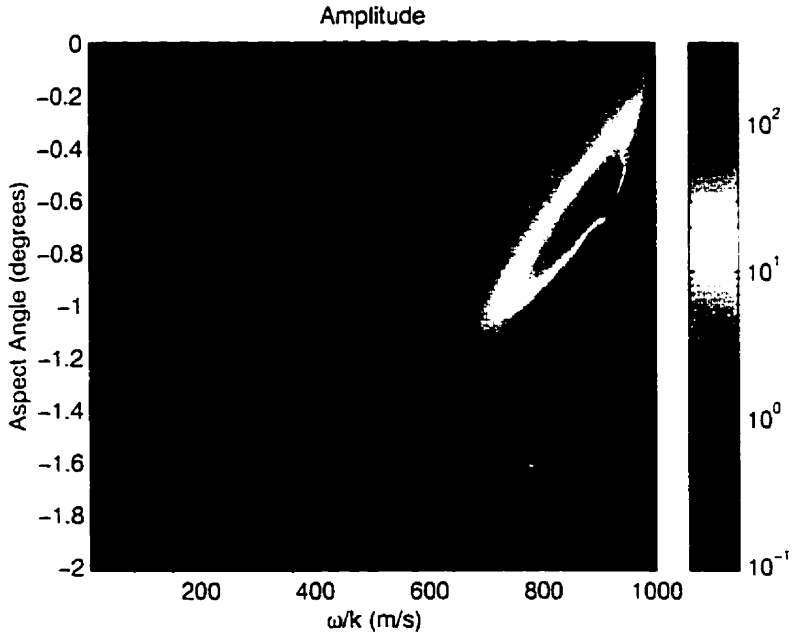

Figure 4.23: Spectrum of phase speeds and aspect angles

the amplitude will change with altitudes and phase speeds respectively altitude and aspect angles. and figure 4.23 predicts how aspect angle and phase speed relate to each other.

To compare these results with the FFT plots. we have to compare figures 4.14 and 4.21 as well as figures 4.15 and 4.19. We can see the expected similarities. but without the spillover problem and low resolution which made the FFT plots relatively useless.

The dark blue areas in the plots indicate that no data is available. or that the amplitude has decayed below the threshold of 10^{-1}.

The striations that are visible in the time plots are an artifact caused by the interpolation technique. but this is not much of a problem since the information in these plots is not something that can be compared with experimental data anyway. they are only included for completeness. The observations will always have some averaging. and the time scales for each wave motion of less than a second are too short to be detected.

One thing to note is that there are two plots for aspect angle versus time. The reason for this is that the original aspect angle plot. i. e. as altitude versus time. does not have unique values for all altitudes. Every aspect angle appears at two different altitudes. one above and one below the minimum. When applying the technique described here. this would lead to a mixture of the two different plots which would confuse the interpolation function and yield nothing useful. Therefore. it had to be split into a part above and below the minimum aspect angle. However. below the minimum there is no growth. both because of a negative growth rate and a divergence of the rays. so that this part of the spectrum does not affect the result.

Figure 4.23 shows that the phase speed does indeed decrease with increasing aspect

angle, as predicted by equation (2.3.2), where Ψ is increasing with the square of the aspect angle.

4.6 Summarized Results

The results from these plots, for the particular conditions set in the program, can be summarized as follows:

1. Waves will converge towards 0.5 degrees aspect angle
2. They will reach the largest amplitude at 0.5 degrees, with significant spread from 0 degrees to 1 degree aspect angle
3. The expected phase speeds are from the ion-acoustic speed of 600 m/s up to the $\mathbf{E} \times \mathbf{B}$ drift of 1000 m/s, with a maximum amplitude at 900 m/s
4. The altitude with significant wave amplitude are from 100 km to 115 km, the maximum being at 110 km.
5. Any particular wave train will evolve within about a second. Traveling upwards at a group velocity of several kilometers per second, it will quickly reach altitudes where the electron-ion drift is no longer sufficient to sustain growth.

Chapter 5

DISCUSSION

5.1 Comparison with Observations

Comparing our results with observations is difficult. The first problem is that the background parameter our model needs, in particular the electric field and the temperatures, are not readily available for the radar observations. Therefore we cannot compare our results to any particular experiment, but have to look at general trends and statistics of the experimental data instead.

Amplitude

The maximum amplitude of our wave train is a factor of about 337 above the noise level. Because the power of radar echoes is proportional to $(\delta n / n_0)^2$, this corresponds to a power level of 50 dB.

Measurements by *Foster et al.* [1992] and *Kustov et al.* [1994] indicate that the scattering cross section of coherent scatter radars like SuperDARN is 50-80 dB stronger than incoherent scatter. However, the problem with the radar measure-

ments is that it is not clear whether the scattering region fills the beam. If it doesn't, the return power will be systematically lower, and this question is still the subject of an ongoing debate.

Even though the frequency of coherent scatter and incoherent scatter is different, this nonetheless shows that our amplitude is quite reasonable.

Altitude

In a recent review, *Sahr and Fejer* [1996] state that the altitude of the echo source is in the lower E region, from 95–125 km. In our results, the power in this region is greater than 20 dB, with a power of 30–50 dB from 105–120 km. We have no growth above 120 km though, but other than that our results agree well with the measurements.

Phase Speed

Apart from the power, the Doppler shift and the equivalent Doppler velocity are probably the best known parameters of the radar echoes. The velocity is therefore often used to categorize the echoes into four types, see for example *Schlegel* [1996] and *Sahr and Fejer* [1996]. In short, type I echoes are characterized by a mean Doppler velocity slightly higher than c_s and a small spectral width of 100–300 m/s and are usually attributed to Farley-Buneman waves. Type II echoes have a small mean velocity but a large width and are believed to be generated by the gradient-drift instability [*Sudan*, 1983]. Type III echoes on the other hand have a small width as well as a small velocity of roughly 0.5 c_s. It is not clear what instabilities generate these echoes. Finally, type IV echoes have a large velocity, much larger than the usual c_s, coupled with a small width. They are not very common, usually seen only

during very disturbed conditions, and are believed to be generated by Farley-Buneman instabilities with an enhanced ion-acoustic speed.

Looking back at figure 4.21 would suggest that our wave train corresponds to a type IV echo because of the large velocity and the relatively small width of roughly 100 m/s at half the maximum. However, our background conditions are not particularly rare, and it seems surprising that type IV echoes are so uncommon if it was indeed the type our wave train would generate.

On the other hand, studies by *Villain et al.* [1987] and *Providakes et al.* [1988] as well as statistical studies by *Hanuise et al.* [1991] and *Lacroix and Moorcroft* [1999] show a clear preference of c_s echoes for coherent radar backscatter experiments.

Thus, with respect to the phase speed, our results do not seem to agree very well with observations, although trying to match the conditions under which radars see c_s echoes could help improving our results.

The reason for this study was in fact the expectation that allowing the waves to travel through the ionosphere would allow them to grow until they reach the threshold speed of c_s, and decay quickly afterwards, so that we expected to see a clear peak at the ion-acoustic speed, which would then be an explanation of the large number of c_s echoes seen with radars. Unfortunately the simulation did not fulfill this expectation.

Aspect Angle

Even though there are measurements with large aspect angles of more than 6° [e.g. *Hofstee and Forsyth*, 1972], most experimental setups observe echoes at a range of aspect angles up to about 2° [*Foster et al.*, 1992], but determining the exact aspect angle is difficult, particularly for HF radars which are subject to refraction, and thus radar beam spread.

Kustov et al. [1994] have studied the variation of the Doppler velocity with aspect angle and have found that the largest velocity to be at 0° aspect angle. The velocity has then decreased to 75% at 0.8°, and to 50% at 1.4°. Comparing these results with figure 4.23 shows a good agreement between our simulation and the measurements.

5.2 Summary

In this thesis I have shown the theoretical background for finding a solution to slowly growing (low frequency) Farley-Buneman waves in a non-uniform medium. I have found a numerically stable and efficient algorithm to solve the resulting differential equations and have shown the results from this calculation. I have also found a way to compute a spectrum of the waves without having to resort to Fourier analysis or Fourier transforms, by combining the knowledge of the local frequency and aspect angle with the amplitude.

A comparison with the observations shows generally good agreement between the simulation and measurements, only the phase speed seems to be too high, that is if compared to type I echoes which we expect to be what our simulation describes. If, on the other hand, we are really simulating type IV echoes, then the phase speed is in good agreement as well.

5.3 Future Work

In view of these results, I propose that the following be studied with this model and the corresponding numerical simulation methods:

Background Effects

It would be useful to study the effects of the background parameters, particularly the electron and ion temperatures and the electric field, on the numerical results. We expect the electron temperature to make a large difference on the spectrum, because it affects the ion-acoustic speed, and with that the phase speed at which the waves would stop growing spontaneously. It also modifies the collision frequencies, and thus the relative electron-ion velocity, which would also have an impact on the results.

Wave Length and Initial Values

The wave length would probably change mostly the maximum amplitude of the results, because it does not affect wave propagation, but the convective effects could have other effects that are not obvious.

The initial aspect angle we have chosen in this study is almost negligible, but it would be useful to examine how it affects the wave evolution. Everything depends on the ray paths which are in turn determined by the aspect angle, so changing the initial value could have a large impact on the results.

Comparison with Observation

In most cases it is difficult to find the real background properties, but by combining the data from several measurement methods, including radars, satellites and rockets, it should be possible to model some of the experiments quite closely, and study how the simulation corresponds to the measurements.

Echo Types

Since type I and type IV echoes seem to be manifestations of the Farley-Buneman instability at different conditions, it would be useful to find out under which conditions our simulation returns an amplitude peak at either c_s for type I echoes or a significantly larger phase speed for type IV echoes.

Comparing these conditions to the real conditions when either type of echoes is detected should prove quite interesting.

Gradient-drift Instability

It should also be possible to include the gradient drift instability into this model. This instability occurs when there is a density gradient in the y direction, and is generally thought to be the origin of type II echoes. Perhaps it is then possible to find conditions under which the simulation returns the properties of any of the four echo types, which could help developing a unified theory which includes all the different types of echoes.

APPENDIX A

SOFTWARE

A.1 Fortran Programs

Programs and Subroutines

This is a description of the Fortran programs used for calculating the numerical solution to this problem.

`main_pro.f`: The main program. It does the calculation of the aspect angle, the ray-tracing and calculates the amplitude as well as all other parameters that change in time.

`nu_elec.f`: Calculates electron temperature and collision frequency profiles

`nu_ion.f`: Calculates ion temperature and collision frequency profiles

`tnden.f`: Reads the MSIS-90 output file and interpolates to the desired altitude resolution

`gridrays.f`: Calculates a regularly spaced grid from the ray-tracing output from `main_pro.f`.

`gridrays_converge.f`: Same as above, but takes the correction due to convergence into account, see equation (3.3.10).

Input files

These files are needed by the above programs for proper execution:

`parameter.F`: File containing all parameters used by `main_pro.f`, including wavelength, electric field and numerical step sizes for example.

`tnden250.dat`: Output from the MSIS-90 model for the neutral temperature and composition

Output files

These files are created by the Fortran programs and are then used as input for making the plots.

`a.dat`: The main output file with amplitude, aspect angle, frequency, spontaneous growth rate, parallel group velocity, and effective growth rate

`rays.dat`: Output from ray-tracing, with altitude and amplitude as well as ω, $k_\parallel$ and ω' interpolated to the ray altitude.

`background.dat`: File with background properties, including temperatures, densities, collision frequencies, Ψ and Ψ', and the velocities in a form easily readable by Matlab

`raygrid.dat`: File created by the ray gridding programs. with a regularly spaced grid created from the ray-tracing output file `rays.dat`.

A.2 Matlab Scripts

Plotting Scripts

These scripts have been used to make the plots presented in this thesis. All scripts have a built-in help text which can be read with the "help" command in Matlab. e. g. "help fbwa".

`init.m`: Initializes the global variables needed by most of these scripts. It in turn needs the file `parameter.m` which is automatically generated by `parameter.awk`. in order to supply Matlab with the background and numerical parameters used in the simulation.

`fbwa.m`: Shows the altitude-time plots from the file `a.dat` as well as ray paths and ray-tracing data from `raygrid.dat`. Plot scales. selection and contour types can be chosen with global variables as described in the help text.

`fbwp.m`: Makes line plots of altitude versus any of the properties in `a.dat`. for selected times.

`showaxissub.m`: Show the plots described in section 4.5. where one axis (or both) has been replaced by the aspect angle or phase speed.

`showbackground.m`: Show a set of plots with background parameters

`showphase.m`: Show plots relating to the phase as well as the Fourier transforms

`showrays.m`: Like `fbwp.m` but for the ray-tracing output

`subplotpart.m`: Split a figure into several subplots. leaving space for footnotes

Helper Scripts

The following scripts are run by the Matlab files mentioned above and are not intended to be used directly:

`goodlegend.m`: Places a legend with the correct size for portrait printing to work around a bug in Matlab's `legend` function.

`imagesc_log_cb.m`: Works similar to Matlab's `imagesc` command, but makes an image with a logarithmic scale and automatically creates the appropriate color bar.

`kpcont.m`: Superimposes contours of the aspect angle on the current plot

`loadrays.m`: Loads the ray-tracing output and prepares it for plotting

`phase.m`: Calculates the phase S by integrating over k

`prepare.m`: Prepares a figure for printing with footnotes describing the simulation properties and the program used to make the plot

`setprint.m`: Adds the footnotes and sets the paper size for printing in letter format

`weighedhistogram.m`: Calculates the plots used by `showaxissub.m` using the method described in section 4.5.

Note that `gridrays.m` has been made obsolete by `gridrays.f` and is no longer needed.

A.3 Supporting Programs

`backup`: Makes an archive of the current run into the tgz file given on the command line. Example: `backup Nov18Run.tgz`

`correctamp.awk`: Obsolete: was needed to correct Fortran output where numbers have an exponent larger than +99. which were a result of the problems with the method of finite differences.

`parameter.awk`: Generates `parameter.m` from `parameter.F` in order to make the parameters in the Fortran program available to Matlab. Should be run as `parameter.awk < parameter.F > parameter.m`

`restore.sh`: Restores an archive made by `backup` and automatically calls the above `parameter.awk` to generate the right Matlab parameter file

A.4 Availability

A CD-ROM with the described programs is available upon request. For further information please contact the author or his supervisor. The email addresses are

Josef Drexler `jdrexler@julian.uwo.ca`

Jean-Pierre St.-Maurice `stmaurice@danlon.physics.uwo.ca`

Alternatively. one can contact the Physics and Astronomy department of the University of Western Ontario. The mailing address is

Department of Physics and Astronomy

University of Western Ontario

London. Ontario. Canada. N6A 3K7

Bibliography

Bretherton, F. P., and C. J. R. Garret. Wave trains in inhomogeneous moving media. *Proc. Roy. Soc. A. 302*. 529–554. 1969.

Buneman, O., Excitation of field-aligned sound waves by electron streams. *Phys. Rev. Lett., 10*. 285–287. 1963.

Chen, D., Convective properties of Farley-Buneman waves at high latitude E-region. Ph.D. thesis. The University of Western Ontario. London. Ontario. Canada. 1996.

Farley, D. T., A plasma instability resulting in field-aligned irregularities in the ionosphere. *J. Geophys. Res., 68*. 6083–6097. 1963.

Foster, J. C., D. Tetenbaum, C. F. del Pozo, J.-P. St.-Maurice, and D. R. Moorcroft. Aspect angle variations in intensity, phase velocity and altitude for high-latitude 34 cm E region irregularities. *J. Geophys. Res., 97*. 8601–8617. 1992.

Greenwald, R. A., W. Weiss, E. Nielsen, and N. R. Thompson. STARE: A new radar auroral backscatter experiment in northern Scandinavia. *Radio Sci., 13*. 1021–1039. 1978.

Greenwald, R. A., K. B. Baker, R. A. Hutchins, and C. Hanuise. An HF phased-array radar for studying small-scale structure in the high-latitude ionosphere. *Radio Sci., 20*. 63–79. 1985.

Hanuise, C., J. P. Villain, J. C. Cerisier, C. Senior, J. M. Ruohoniemi, R. A. Greenwald, and K. B. Baker, Statistical study of high-latitude E-region doppler spectra obtained with the SHERPA HF radar. *Ann. Geophys., 9*. 273–285. 1991.

Hedin, A. E., Extension of the MSIS thermospheric model into the middle and lower atmospheres. *J. Geophys. Res., 96*. 1159–1172. 1991.

Hofstee, J., and P. A. Forsyth. Ion-acoustic waves and aspect sensitivity in radio aurora. *J. Atmos. Terr. Phys., 34*. 893–902. 1972.

Kustov, A. V., M. Uspensky, G. J. Sofko, J. A. Koehler, and J. Mu, Aspect angle dependence of the radar aurora doppler velocity. *J. Geophys. Res., 99*. 2131–2144. 1994.

Lacroix, P., and D. R. Moorcroft. Ion acoustic E region echoes from near the cusp. in *Proceedings of the SuperDARN Annual Meeting*. p. 35. 1999.

Providakes, J., D. T. Farley, B. G. Fejer, J. Sahr, and W. E. Swartz, Observations of auroral E-region plasma waves and electron heating with EISCAT and a VHF radar interferometer. *J. Atmos. Terr. Phys., 50*. 339–356. 1988.

Sahr, J. D., and B. G. Fejer, Auroral electrojet plasma irregularity theory and experiment: A critical review of present understanding and future directions, *J. Geophys. Res.*, *101*, 26,893–26,909, 1996.

Schlegel, K., Coherent backscatter from ionospheric E-region plasma irregularities, *J. Atmos. Terr. Phys.*, *58*, 933–941, 1996.

Schlegel, K., and J.-P. St.-Maurice, Anomalous heating of the polar E-region by unstable plasma waves, 1, Observation, *J. Geophys. Res.*, *86*, 1447–1452, 1981.

St.-Maurice, J.-P., A nonlocal theory of the high-latitude Farley-Buneman instability, *J. Geophys. Res.*, *90*, 5211–5225, 1985.

St.-Maurice, J.-P., K. Schlegel, and P. M. Banks, Anomalous heating of the polar E-region by unstable plasma waves, 2, Theory, *J. Geophys. Res.*, *86*, 1453–1462, 1981.

St.-Maurice, J.-P., et al., New insights from a nonlocal generalization of the Farley-Buneman instability problem at high latitudes, work in progress.

Sudan, R. N., Unified theory of type I and type II irregularities in the equatorial electrojet, *J. Geophys. Res.*, *88*, 4853–4860, 1983.

Villain, J. P., R. A. Greenwald, K. B. Baker, and J. M. Ruohoniemi, HF radar observations of E region plasma irregularities produced by oblique electron streaming, *J. Geophys. Res.*, *92*, 12,327–12,342, 1987.